atmosphere

MDPI

Article

Intelligent Identification and Verification of Flutter Derivatives and Critical Velocity of Closed-Box Girders Using Gradient Boosting Decision Tree

Neyu Chen [1], Yaojun Ge [1,*] and Claudio Borri [2]

[1] State Key Lab of Disaster Reduction in Civil Engineering, Tongji University, Shanghai 200092, China; chenneyu@tongji.edu.cn
[2] Department of Civil and Environmental Engineering, University of Florence, 50139 Florence, Italy; claudio.borri@unifi.it
* Correspondence: yaojunge@tongji.edu.cn

Abstract: Flutter derivatives (FDs) of the bridge deck are basic aerodynamic parameters by which flutter analysis determines critical flutter velocity (CFV), and they are traditionally identified by sectional model wind tunnel tests or computational fluid dynamics (CFD) numerical simulation. Based on some wind tunnel testing results and numerical simulation data, the machine learning models for identifying FDs of closed-box girders are trained and developed via a gradient boosting decision tree in this study. The models can explore the underlying input–output transfer relationship of datasets and realize rapid intelligent identification of FDs without wind tunnel tests or numerical simulation. This method also provides a convenient and feasible option for expanding datasets of FDs, and the distribution of FDs can be analyzed through the post-interpretation of trained models. Combined with FD sensitivity analysis, the models can be verified by the calculation error of CFV. In addition, the proposed method can help determine the appropriate shape of the box girder cross-section in the preliminary design stage of long-span bridges and provide the necessary reference for aerodynamic shape optimization by modifying the local geometric features of the cross-section.

Keywords: flutter derivative; intelligent identification; closed-box girder; machine learning; gradient boosting decision tree; sensitivity analysis

Citation: Chen, N.; Ge, Y.; Borri, C. Intelligent Identification and Verification of Flutter Derivatives and Critical Velocity of Closed-Box Girders Using Gradient Boosting Decision Tree. *Atmosphere* **2023**, *14*, 1165. https://doi.org/10.3390/atmos14071165

Academic Editors: Bowen Yan, Jinhui Yan, Chao Li, Chaorong Zheng, Xiao Li and Qiusheng Li

Received: 1 June 2023
Revised: 16 July 2023
Accepted: 17 July 2023
Published: 18 July 2023

1. Introduction

With rapid advancements in the building materials and construction techniques over recent years, there has been an upward trend in the number of long-span bridges being proposed to cross wide canyons, rivers, and straits [1]. Long-span bridges are characterized by lighter weight, higher flexibility, and lower damping; hence, they are vulnerable to wind effects and usually dominated by the wind-resistant performance in the structural design process. To describe the wind-resistant performance of the bridge structure, the aerodynamic parameters related to various wind-induced vibrations of the bridge girder need to be identified. They play a vital role in the analysis of the wind-induced static stability, flutter, vortex-induced vibration, and buffeting of the bridge. Among them, flutter instability, which would activate violent oscillations and could result in the collapse of bridge structures, should be prevented at all times.

In order to predict the flutter performance of bridge deck sections, the identification of flutter derivatives (FDs) is the most critical step. Currently, the FDs can be well identified using wind tunnel tests or numerical simulation based on computational fluid dynamics (CFD). Based on the vibration state of the sectional model, there are three methods of identifying FDs in the wind tunnel tests: forced vibration [2]; free vibration [3]; and random vibration [4]. Each of these methods can be divided into two types: time domain and frequency domain. The coupled free vibration method has commonly been the preference to

extract the bridge FDs in wind tunnel tests due to its instrumental simplicity and operational convenience [5–7]. A series of methods were developed over the past several decades based on the free decay time histories of the bridge deck at various wind speeds [8,9]. CFD methods can achieve numerical calculations for various fluid problems by solving fluid control equations. Numerical tests require an adequate load model with a turbulent stochastic structure and a suitable structural model for each bridge in order to describe the wind action [10]. Borri et al. established multiple wind load models for time-domain simulation of the wind-induced vibration of bridges [11,12]. Fang et al. modeled and simulated extreme winds and their effects in different ways [13,14]. Similar to the wind tunnel test, all the identification methods for FDs can be also achieved by CFD [15–17]. At present, the numerical identification of FDs is mainly based on the sub-state forced vibration method: the structure is forced to vibrate at a certain frequency in the single DoF. Aerodynamic forces can be obtained, and the least square method is used for the exaction of FDs.

Although the wind tunnel test is considered to be the most effective and reliable means for the FD identification of bridges, and the advancement of computer capacity enables more rapid simulation of CFD, many aspects of these traditional research methods still face challenges. Traditional wind tunnel tests have the issue of high cost and can only be used to analyze specific bridge decks. The experimental results are not universal since these aerodynamic parameters are bridge-deck-dependent. For numerical simulation, the process still requires a large amount of computational resources to reach a high precision. Although CFD analysis has its potential, certain characteristics of bluff body flutter are not yet completely understood (for example, turbulence), and there still remain great challenges to modeling the phenomenon solely by numerical simulation. In recent years, as an advanced alternative technique, machine learning has provided a novel solution for the identification of aerodynamic parameters and the wind-resistant performance analysis of bluff body sections. Machine learning is a technique of data science that helps computers learn from existing data to forecast unknown behaviors, outcomes, and trends. There are already some mature open-source wind engineering databases, which have mainly been established by wind engineering groups from Canada, China, Japan, the USA, etc. Zhou and Kareem first established an online aerodynamic database for tall buildings in 2003 (http://aerodata.ce.nd.edu/) (accessed on 1 September 2022) [18]. Wang and Cheng conducted high-frequency force balance wind tunnel tests on more high-rise building models and built a wind resistance database for them based on the expert system (http://windexpert.ce.tku.edu.tw/) (accessed on 1 September 2022) [19]. In terms of an aerodynamic database for low-rise buildings, Ho and Kopp built the NIST aerodynamic database from a large number of pressure measuring tests of low-rise building models conducted at the University of Western Ontario [20]. Quan and Tamura developed a publicly accessible database of surface wind pressure for low-rise buildings (http://www.wind.arch.t-kougei.ac.jp/info_center/weic.html) (accessed on 1 September 2022) [21]. The existence of these data and databases is a prerequisite for researchers to carry out wind resistance analysis using machine learning methods.

In the past 20 years, machine learning methods have been successfully applied to the identification of aerostatic coefficients and flutter derivatives (FDs), as well as to the analysis of wind-resistant stability. Jung et al. took the lead in realizing the estimation of six FDs of a rectangular section using an artificial neural network (ANN) based on 17 sets of experimental data [22]. The ANN was utilized by Chen et al. to predict eight FDs of bluff body sections [23]. The support vector machine (SVM) was introduced by Lute et al. to identify FDs of the main girder before estimating the critical flutter velocity (CFV) of cable-stayed bridges [24]. Chung et al. used CFD simulations and the forced vibration test in a wind tunnel to estimate eight FDs of a rectangular section by the back propagation neural network (BP neural network) [25]. The ANN model based on the Levenberg–Marquardt algorithm was derived and trained using various geometrical and mechanical parameters of the bridge deck cross-section, and CFV of suspension bridge with

closed box deck sections can be predicted directly [26]. Abbas et al. used the normalized lift force and torsional moment coefficients at current time step as the output of ANN to predict the aeroelastic response of bridge decks [27]. Mei proposed a machine learning strategy for flutter prediction based on four widely used machine learning algorithms [28]. Li et al. applied ANNs to establish the relationship between aerostatic coefficients and flutter performance for fast prediction of CFV [29]. All these studies confirm the feasibility and effectiveness of machine learning methods in the FDs identification and flutter performance analysis [30]. However, these attempts are not really independent of specially designed wind tunnel tests. Current research lacks the integration and data-mining of the existing results of wind tunnel tests or numerical simulations. Furthermore, most of the existing research describes a direct application of common machine learning methods to a specific scenario in parameter identification or wind resistance analysis without illustrating the applicability of the algorithms and improving them accordingly. The existing machine learning applications are mostly employed to build a black box, lacking the interpretation and extension of the identification model.

The objective for this paper is to utilize previously measured experimental results that contain invaluable information about flutter mechanics. Approximations based on the cumulated existing data are expected to produce acceptable results, and imprecision tolerance of the gradient boosting decision tree (GBDT) is a beneficial characteristic when solving the problems of parameter identification without big data. In this study, the FDs of closed-box girders are trained and predicted by GBDT based on a specialized bridge wind resistance performance database, and the prediction results are applied to the related analysis of flutter performance. Figure 1 shows the technology roadmap of this study.

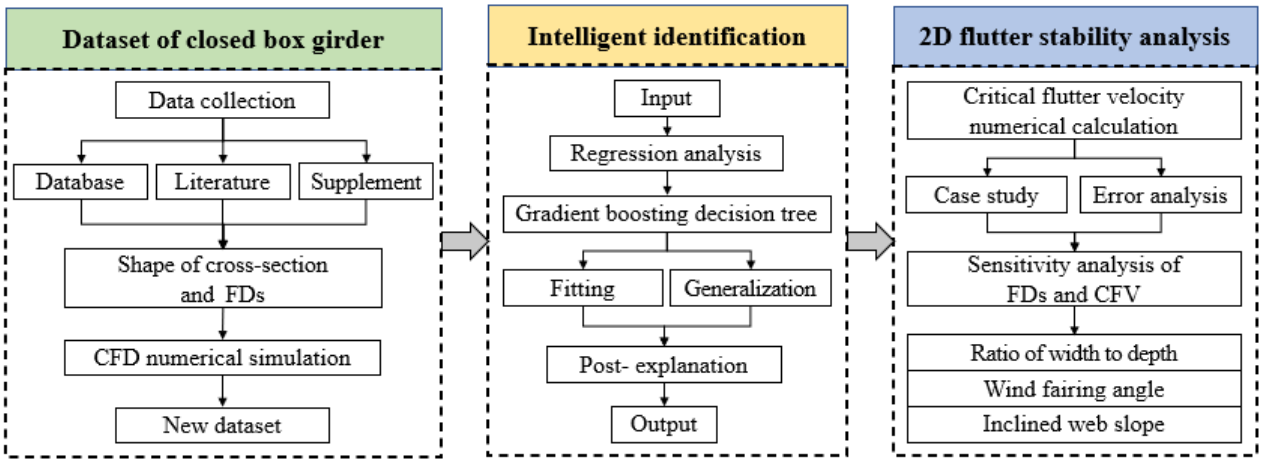

Figure 1. Technology roadmap.

2. Identification Methods of Flutter Derivatives

This section introduces the traditional identification methods for FDs. It begins with physical identification, including the theoretical definition of FDs and the wind tunnel test measurement methods. This is followed by numerical identification, i.e., numerical simulation by CFD methods to extract the FDs.

2.1. Physical Identification

For a bridge deck that is immersed in the incoming air flow, the oscillation was mainly driven by the self-excited force. The mechanical system of flutter is described by a two degrees of freedom (DoFs) linear oscillator, free to vibrate in heaving $h(t)$ and pitching $\theta(t)$ modes, as shown in Figure 2 (where U represents the incoming wind speed; L and M represent self-excited lift force and torque, respectively).

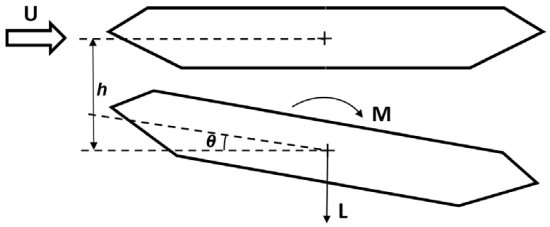

Figure 2. Reference system for displacements and self-excited forces.

Based on the study performed by Scanlan and Tomko, the wind-induced linear self-excited force on a bridge deck is modeled as the function of the vibration state, i.e., displacements and velocities in two DoFs using eight FDs [31]:

$$\begin{aligned} L_{se} &= \tfrac{1}{2}\rho U^2 B\left[KH_1^*\tfrac{\dot{h}}{U} + KH_2^*\tfrac{B\dot{\theta}}{U} + K^2H_3^*\theta + K^2H_4^*\tfrac{h}{B}\right], \\ M_{se} &= \tfrac{1}{2}\rho U^2 B^2\left[KA_1^*\tfrac{\dot{h}}{U} + KA_2^*\tfrac{B\dot{\theta}}{U} + K^2A_3^*\theta + K^2A_4^*\tfrac{h}{B}\right] \end{aligned} \quad (1)$$

where U is the wind speed; ρ is the air density; B is the width of the bridge deck; K is the $\omega B/U$ which is the reduced frequency of oscillation; ω is circular frequency of the coupled mode; and H_i^* and A_i^* (i = 1,2,3,4) are the FDs.

In this study, the unifying least square method developed by Gu et al. [32] and improved by Ding et al. [6], Li et al. [33] and Bartoli et al. [34] was utilized to extract the FDs in wind tunnel tests, which was referred to as the modified unifying least square (MULS) approach.

2.2. Numerical Identification

The FDs calculated by CFD numerical simulation in this paper are based on the forced vibration method. It avoids solving the motion equation, which saves time and is easy to be realized by software (ANSYS Fluent 2021 R1). The two degrees of freedom of cross-section motion are decoupled, and the model is designated to perform vertical and torsional motions respectively. Based on Scanlan's theoretical framework of the superposition of linear self-excited forces, it is assumed that the model performs multi-frequency forced vibration of a single degree of freedom:

$$\begin{cases} h(t) = \sum_{i=1}^{n} h_0 \sin(2\pi f_i t) \\ \alpha(t) = \sum_{i=1}^{n} \alpha_0 \sin(2\pi f_i t) \end{cases}, \quad (2)$$

where h_0 and α_0 are the vertical bending and torsional amplitudes. The FDs are obtained by identifying the amplitude of aerodynamic force and the phase difference between force and displacement through the frequency domain method.

3. Intelligent Identification of Flutter Derivatives

The machine learning algorithm applied to predict the FDs is introduced in this section. Typical machine learning methods mainly include decision trees, random forests, artificial neural networks, and Bayesian learning. In the case of big data, the accuracy that can be achieved by existing machine learning methods shows insignificant difference. However, in the face of a small amount of data, it is necessary to compare various machine learning algorithms before selecting the most favorable one. The comparison of various algorithms has been performed in our previous study [35], showing that the error back propagation (EBP) neural network presents serious danger of falling into local minimum since it is based on a gradient descent method. Support vector regression (SVR) requires very rigorous data pre-processing and hyperparameters tuning, so the model is difficult to check and adjust. Gradient boosting decision tree (GBDT) has the advantages of good training effect and less overfitting on low-dimensional data, and its framework allows post-interpreters to be run for model representation and improvement.

A hybrid model combining GBDT and the linear regression method is therefore used for the training of FDs in this study. Its main idea is to use weak classifiers (decision trees) to iteratively train input data before obtaining the optimal model. The architecture of the model is shown in Figure 3. Input features are transformed by means of GBDT which consists of m decision trees. The number of trees and the number of branches and leaf nodes per tree are determined based on the amount of input data. In the construction of the decision tree, if it cannot further improve the generalization ability of the model, the creation of leaf nodes will be stopped. To avoid overfitting, a threshold can also be set to limit the creation of leaf nodes, which is called to pre-pruning. After successfully constructing a complete decision tree, the sub-trees can be checked by replacing them with leaf nodes; then, the sub-trees will be replaced if the model can be improved with leaf nodes, which is called post-pruning. During the whole training process of GBDT, a new tree is added to the existing trees to reduce the residuals of the current model in the gradient direction, and the negative gradient of the loss function is taken as the approximate value of the residual to replace the residual. Finally, the transformed features w_i ($i = 0, 1, 2, \ldots, n$) are trained in a linear regression model to obtain the final prediction results.

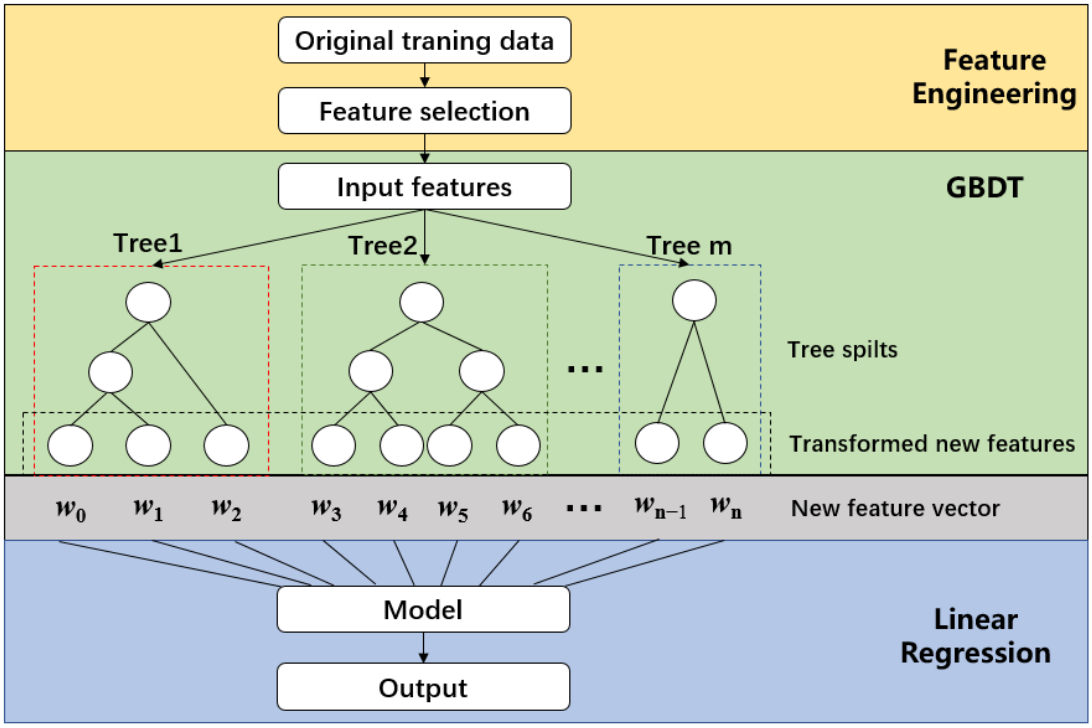

Figure 3. Architecture of GBDT.

3.1. Negative Gradient Fitting

GBDT is one of the widely used models under the gradient boosting framework. It accomplishes the task of classification by defining a logarithmic loss function for logistic regression. To solve the problem of measuring the approximation of the loss function, the gradient boosting algorithm uses the negative gradient of the loss function to fit the approximation of the loss and fits a classification and regression tree (CART) so that the loss in each round becomes as small as possible.

The minimum value of the loss function is:

$$C_{mj} = \text{argmin} \sum L(y_i, f_{m-1}(x_i) + c) \ (x \in R_{mj}), \tag{3}$$

where the function L is a logarithmic loss function; x_i is the eigenvalue of the input; y_i is the output; and c is a constant. R_{mj} is the zone of the decision tree j domain; and i, m, j are counting variables.

The decision tree fitting function is:

$$h_m(x) = \sum_{j=1}^{J} C_{mj} I(x) \quad (x \in R_{mj}), \tag{4}$$

where the function $I(x)$ is an indicator function that returns 0 when the equation in parentheses is false; otherwise, it returns to 1. J is the number of iterations.

The updated boosting decision tree is the sum of the previously fitting decision trees and the latest fitting function:

$$f(x) = f_{m-1}(x) + h_m(x). \tag{5}$$

3.2. GBDT Regression

GBDT can be used for classification and regression, and the principles of both are similar. A weak learner is generated in each round, and a strong predictive model is achieved through continuous accumulation. Based on the above definitions of negative gradient loss function and update process, the entire GBDT regression process is expressed as follows.

1. Initialize loss function:

$$f_0(x) = \text{argmin} \sum_{i=1}^{N} L(y_i, c) = \frac{1}{2} \log \frac{1+\overline{y}}{1-\overline{y}}, \tag{6}$$

where $f_0(x)$ is the initial value of the algorithm; N denotes the length of the training set; $\overline{y}$ represents the mean of outputs; and the others are defined as above.

2. For each number of iteration rounds, $m = 1, 2, \ldots, M$.

For the training set ($i = 1, 2, \ldots, N$,) compute the negative gradient which is also the residual r_{mi}:

$$r_{mi} = -\left[\frac{\partial L(y_i, f(x_i))}{\partial f(x_i)}\right]_{f(x)=f_{m-1}(x)}. \tag{7}$$

3. Fit a decision tree with r_{mi}, obtain the leaf node region R_{mj} of the m-th tree.

For $j = 1, 2, \ldots, J$, use linear search to obtain the minimum value of loss function:

$$C_{mj} = \text{argmin} \sum L(y_i, f_{m-1}(x_i) + c) \ (x \in R_{mj}). \tag{8}$$

4. Update $f(x)$:

$$f(x) = f_{m-1}(x) + \sum_{j=1}^{J} C_{mj} I(x) \ (x \in R_{mj}). \tag{9}$$

3.3. Algorithm Optimization

The GBDT model has the advantages of robustness, applicability to low-dimensional problems, and fast tuning. In the case of small samples, GBDT has poor generalization and usually faces the problem of overfitting. To solve this issue, a regular term is added to the original loss function to improve the generalization of the trained model. The loss function after adding the regular term is shown as follows:

$$L' = \sum_{n=1}^{N} L(y_i, f_{m-1}(x_i) + c) + \sum_{m} \Omega(g_m), \tag{10}$$

where $\Omega(g) = \delta T + \frac{1}{2}\lambda \|w\|^2$; δ and λ are hyperparameters; T is the number of leaf nodes; and w is a vector consisting of all leaf node values.

4. Datasets and Data Processing for Intelligent Identification

This section begins with the introduction of a specialized wind resistance performance database for long-span bridges. Next, two types of datasets for intelligent identification of FDs are presented, including hybrid datasets and pure numerical simulation datasets. The selection of wind tunnel test data from the database, the collected numerical simulation data from literature, and the supplementary data in the hybrid datasets are introduced. Then, the pure numerical simulation datasets obtained through CFD recalculation are described.

4.1. Bridge Wind Resistance Performance Database

Although there are some mature open-source wind engineering databases in the world, these databases are all specific to building structures and are self-contained. Even if they can be used for bridge wind resistance, the data types may not be matched completely. Therefore, a specialized bridge wind resistance performance database is developed in this study before performing the machine learning of parameters of interest. This database collected the test data of nearly 100 long-span bridges from the wind tunnel laboratory of Tongji University since a large quantity of wind tunnel test data for long-span bridges have been accumulated at Tongji University up to now, and various experimental data have been unified to the same criterion.

This database uses Microsoft Access as the underlying database system. To facilitate the users' visual operation, the Java programming language is adopted to establish the foreground application interface. The connection between the underlying database and the foreground application is driven by a local protocol to achieve platform independence and high execution efficiency [36]. After classification, all the data are summarized into three modules: basic information; dynamic characteristics; and aerodynamic parameters. The basic information includes the type of bridge, span, the material of girder, the type and size of cross-section, mass, stiffness, basic wind speed, critical velocity, amplitude, etc. The dynamic characteristics include the natural frequency and mode of vibration of each bridge. Aerodynamic parameters include the aerostatic coefficients and flutter derivatives (FDs), but aerodynamic admittance is not involved.

4.2. Closed-Box Girder Dataset

This subsection introduces the hybrid datasets of closed-box girders, which include 20 sets of wind tunnel test data from the database, 20 sets of collected numerical simulation data from the open-source literature, and 14 sets of supplementary data.

4.2.1. Physical Identification Data through Wind Tunnel Tests

Specifically, FDs and the flutter performance of bridges using closed-box girder are extracted and studied. For machine learning modeling, it is necessary to establish a specialized sample set of closed-box girders, including the dimensions of the cross-section, the wind attack angle, the reduced wind velocity, FDs, etc. The wind tunnel test data of 20 long-span bridges with streamlined closed-box girders are selected from the database as mentioned above. The specific involved parameters include the dimensions of cross-section, the FDs under different reduced wind velocities, and the airflow field conditions of wind tunnel tests. The dimensions of the cross–section are shown in Figure 4, including the width of deck—B, box height of beam—H, wind fairing extension length—b, wind fairing angle—α, and inclined web slope—β. These five parameters can determine the unique closed-box girder section, and they are independent of each other. The specific dimensions of these 20 sets of cross-sections are illustrated in Table 1, and the FDs of these 20 sets of cross-sections are given in Figure 5.

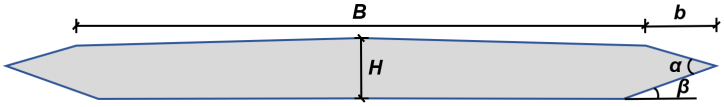

Figure 4. Architecture of a closed-box girder.

Table 1. Geometric size of 20 sets of cross-sections collected for wind tunnel test.

Section No.	B (m)	H (m)	b (m)	α (°)	β (°)
1	35.2	3.535	1.79	40	15
2	28.5	3.0	0.97	60	8
3	30.0	3.5	2.0	39	14
4	46.7	5.83	1.66	63	18
5	40.8	3.5	0.6	72	13
6	33.5	2.875	2.9	50	20
7	36.2	3.8	0.9	71	20
8	40.0	3.74	2.25	48	21
9	45.2	3.0	1.15	64.8	18.6
10	43.0	2.0	1.0	55.8	10.8
11	30.0	5.0	5.5	49	24
12	36.9	3.6	1.0	66	14
13	43.0	3.0	1.0	62	16
14	30.4	3.5	0.6	73	23
15	18.0	2.5	1.8	48	22
16	50.0	2.5	0.8	60	10
17	44.0	4.5	1.0	79	26
18	33.5	3.0	1.7	48.1	19.9
19	38.0	4.0	1.3	59	15
20	28.6	3.5	0.7	72.6	17.6
Range	18.0–50.0	2.0–5.8	0.6–5.5	39–79	8–26

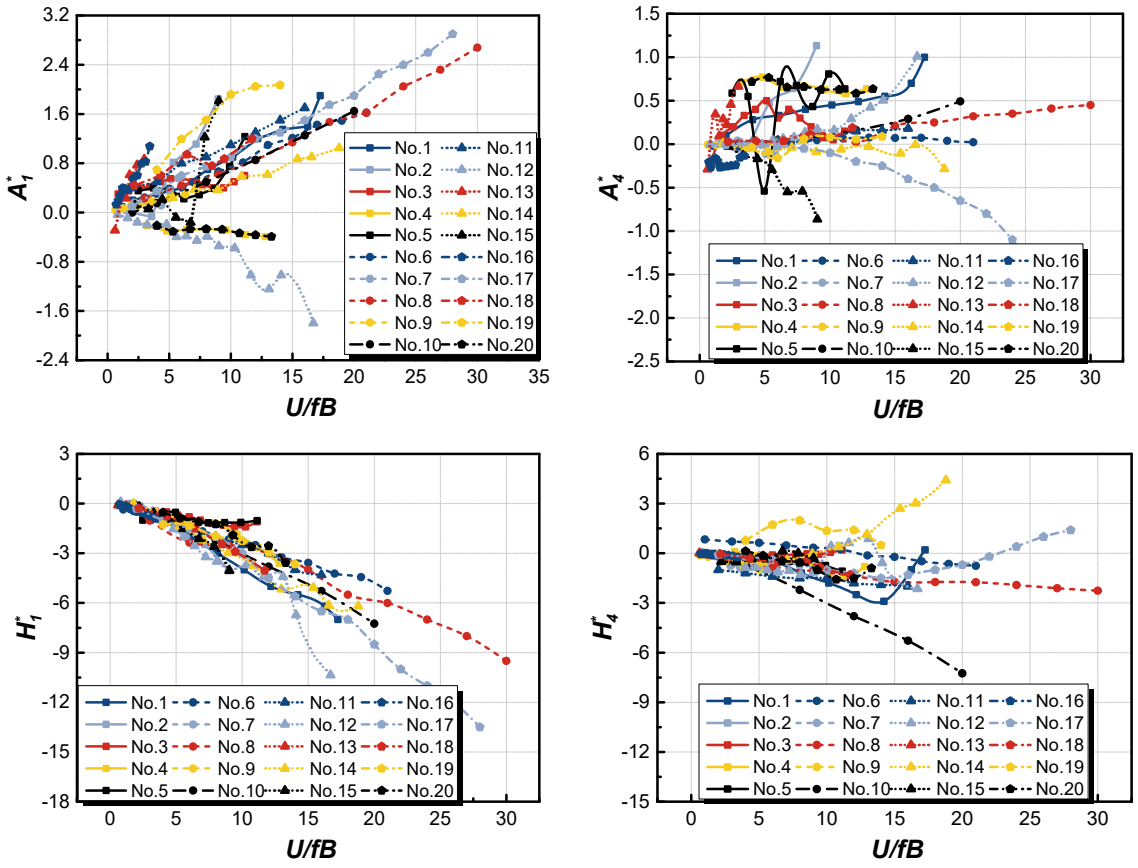

Figure 5. *Cont.*

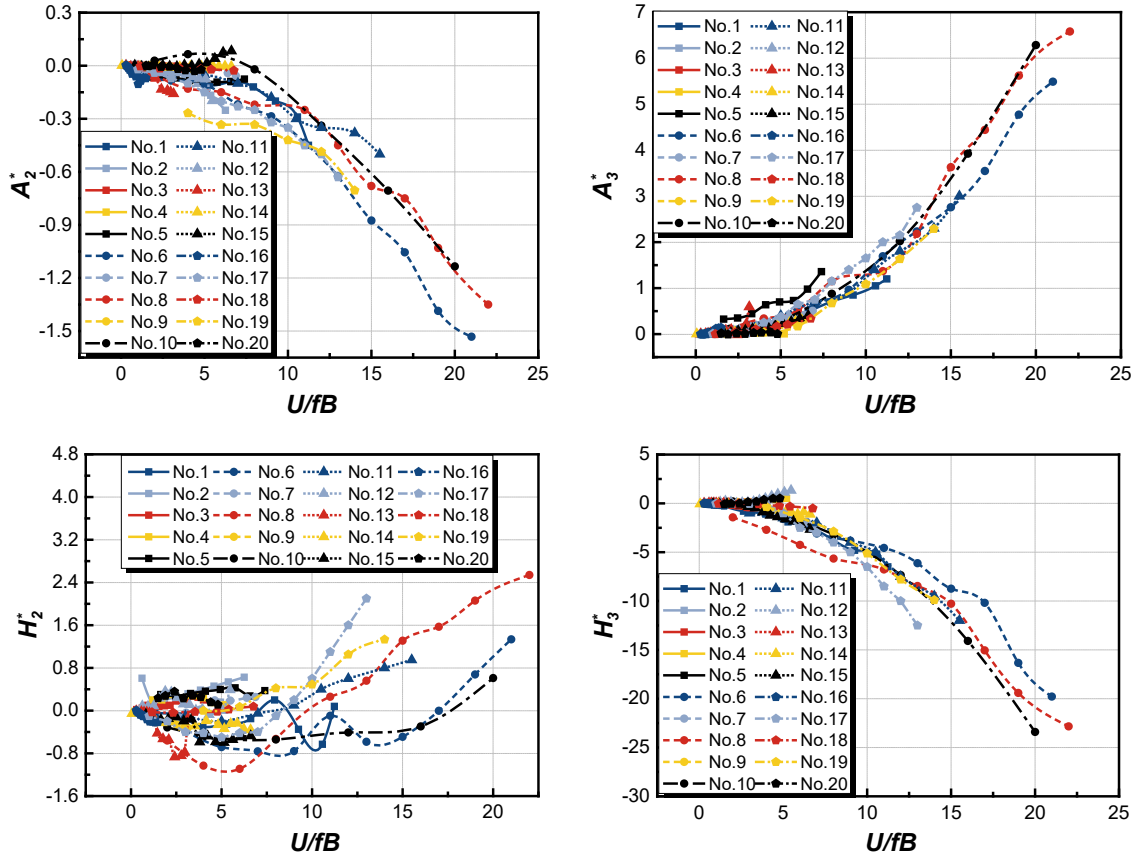

Figure 5. 8 FDs under different reduced wind speeds of 20 sets of cross-sections from database.

4.2.2. Numerical Identification Data Based on CFD Simulation

To improve the machine learning effect, another 20 sets of numerical simulation data for closed-box girders from open-source literature were added as mixed datasets to jointly drive the training process of machine learning. The involved parameters are consistent with the wind tunnel test data. The specific dimensions of these 20 sets of data are illustrated in Table 2, and the FDs of these 20 sets of cross-sections are given in Figure 6.

Table 2. Geometric size of the collected 20 sets of cross-sections for numerical simulation.

Section No.	B (m)	H (m)	b (m)	α (°)	β (°)
21 [37]	38.5	4.39	1.25	65.3	12.26
22 [38]	33.9	3.0	1.8	47.7	21.14
23 [39]	12.0	2.0	0.9	50.8	22.2
24 [40]	29.7	3.9	0.15	101.4	17.84
25 [41]	27.0	4.3	2.0	53.6	27.1
26 [42]	45.2	3.1	2.44	36.4	9.8
27 [43]	35.5	3.5	3.1	34.7	18.5
28 [44]	29.9	3.0	0.8	79.1	19.95
29 [45]	26.0	2.8	1.7	40.9	15.7
30 [46]	35.5	3.5	2.18	44	21
31 [47]	35.0	3.5	1.8	48.6	20.77
32 [48]	41.0	3.5	0.5	76.7	13.12
33 [49]	23.2	3.36	1.92	48.1	19.28
34 [50]	35.3	3.54	4.2	30	15.6
35 [51]	45.2	3.0	1.152	65	19
36 [52]	31.1	2.8	1.8	43.1	16.5
37 [53]	39.0	2.0	3.0	37	18
38 [54]	38.0	3.5	1.3	59.1	17.2
39 [55]	35.5	3.54	3.12	38.2	18.15
40 [56]	35.9	3.5	1.3	59.5	11.42
Range	12.0–45.2	2.0–4.39	0.15–4.2	30–101.4	9.8–27.1

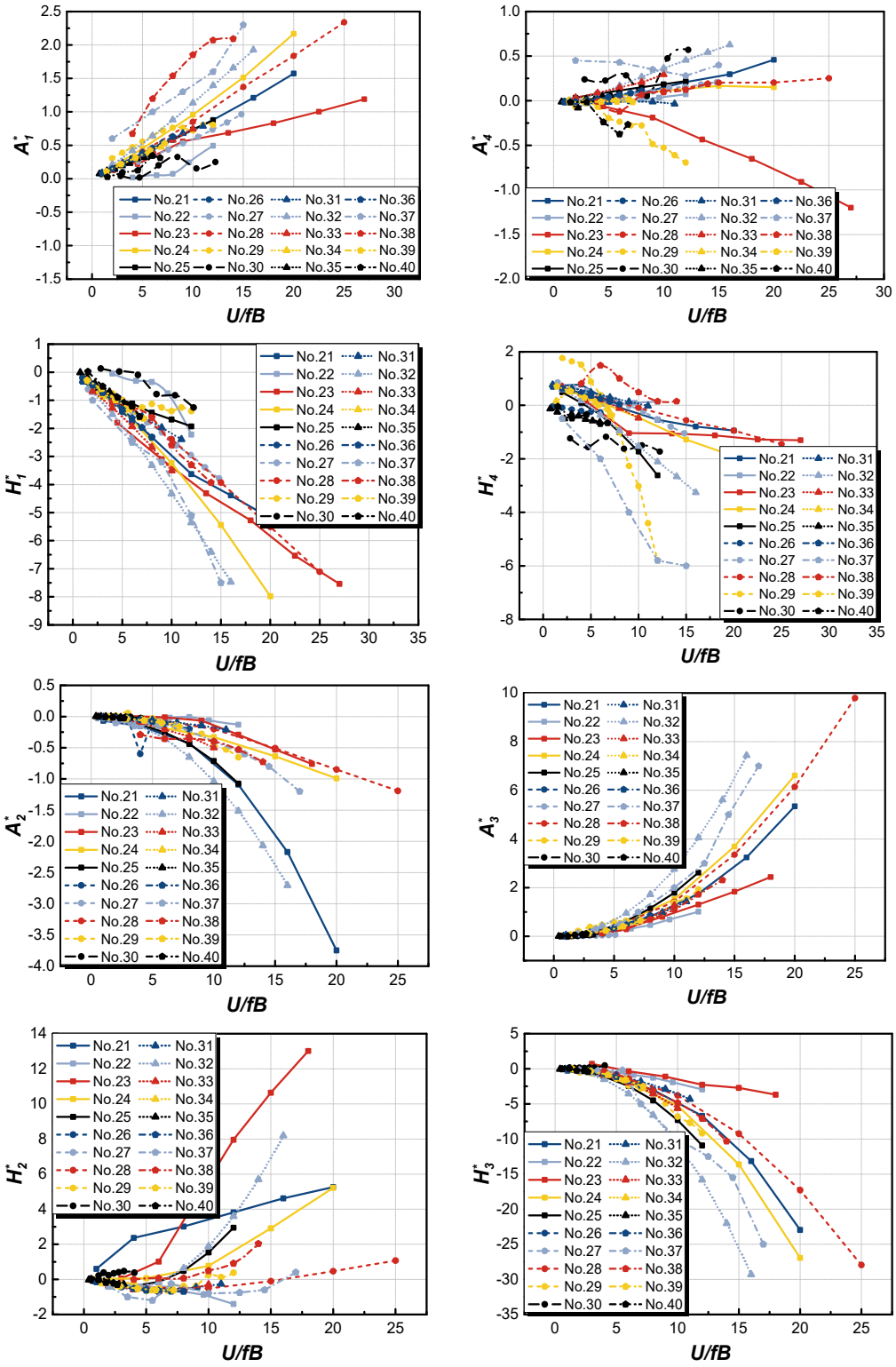

Figure 6. 8 FDs under different reduced wind speeds of 20 sets of cross-sections from literature.

4.2.3. Supplementary Data

This study focuses on the machine learning prediction of flutter derivatives and flutter performance of closed-box girders. The value range of shape parameters of the cross-sections in the sample set will have a decisive impact on the prediction results. The existing 40 sets of data are not uniform in terms of dimensions such as the width and height, etc., of the cross-section. Moreover, considering the actual requirements of the bridge

structure, each aerodynamic shape parameter has a concentrated distribution range, so the representativeness of the existing data is also not good enough. For example, most of the wind fairing angles used in projects are between 45° and 60°. Most of the inclined web slopes are between 15° and 25°, and 11° and 32° are also often used in engineering [57]. Based on the above considerations, an additional 14 sets of cross-sections were added in this study, whose size distributions remain within these concentrated distribution ranges and fill in the gaps in some size ranges. The specific dimensions of these 14 sets of supplementary data are illustrated in Table 3, and the FDs of these 14 sets of cross-sections are given in Figure 7 by CFD numerical simulation. Therefore, a total of 54 sets of closed-box girder cross-sections form a complete sample set for machine learning training. The distribution of the whole sample set tends to be closer to a Gaussian distribution than a uniform distribution, as shown in Figure 8, with the aim of making subsequent machine learning applications more engineering-practical.

Table 3. Geometric size of 14 sets of supplementary cross-sections.

Section No.	B (m)	H (m)	b (m)	α (°)	β (°)
41	30.5	3.0	1.7	57	28
42	29.5	3.0	1.5	57	17
43	34.3	3.2	1.5	50	13
44	26.2	2.8	0.7	70	20
45	25.5	3.0	1.5	51	19
46	51.4	5.0	1.5	57	14
47	54.0	5.8	2.0	65	15
48	32.8	3.2	0.6	60	12
49	39.1	4.6	2.1	53	23.5
50	42.8	4.5	2.0	53	17.5
51	41.8	4.4	2.0	53	16.5
52	58.1	4.3	1.9	43	16.5
53	56.7	4.2	1.9	43	11.5
54	59.5	4.1	1.8	37	16.5
Range	25.5–59.5	2.8–5.8	0.6–2.1	37–70	12–28

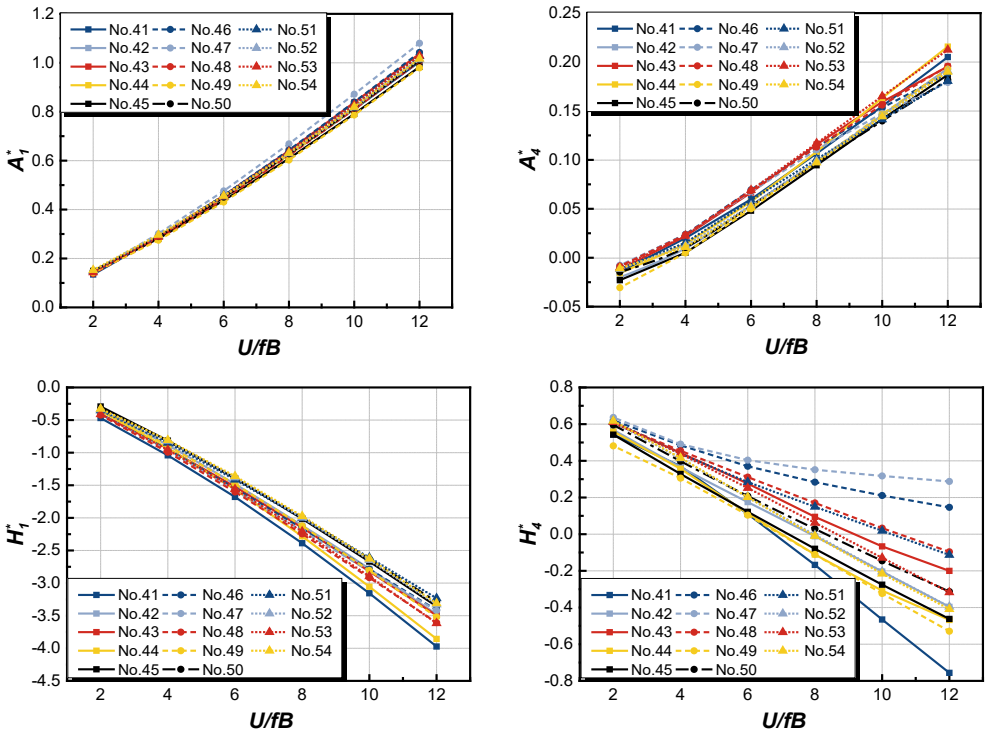

Figure 7. *Cont.*

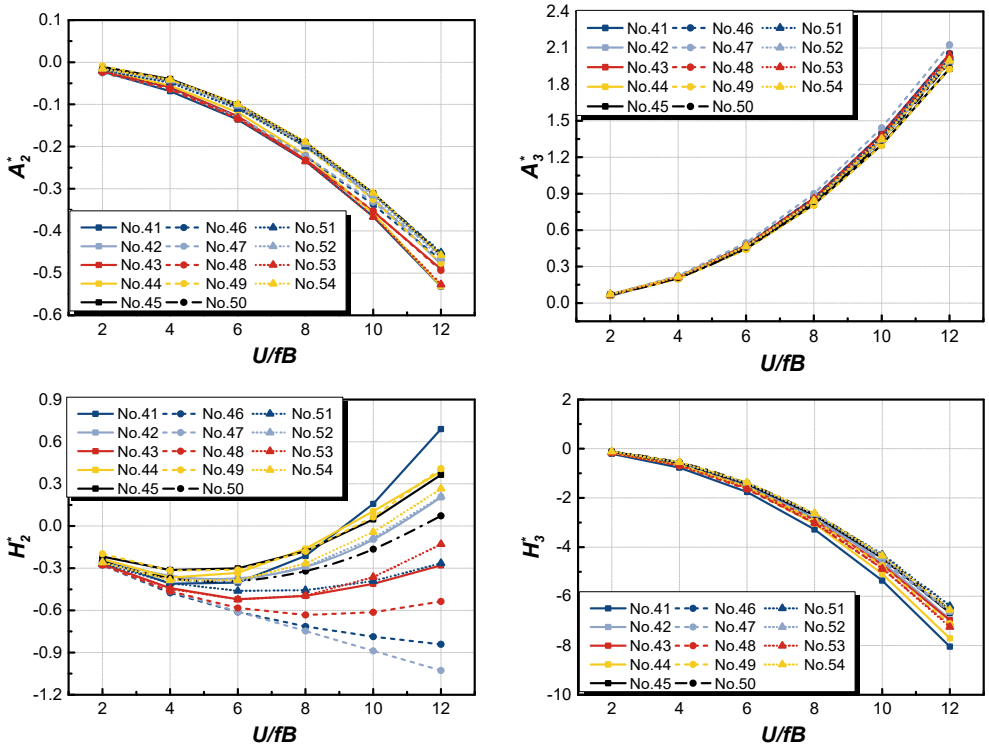

Figure 7. 8 FDs under different reduced wind speeds of 14 sets of supplementary cross-sections.

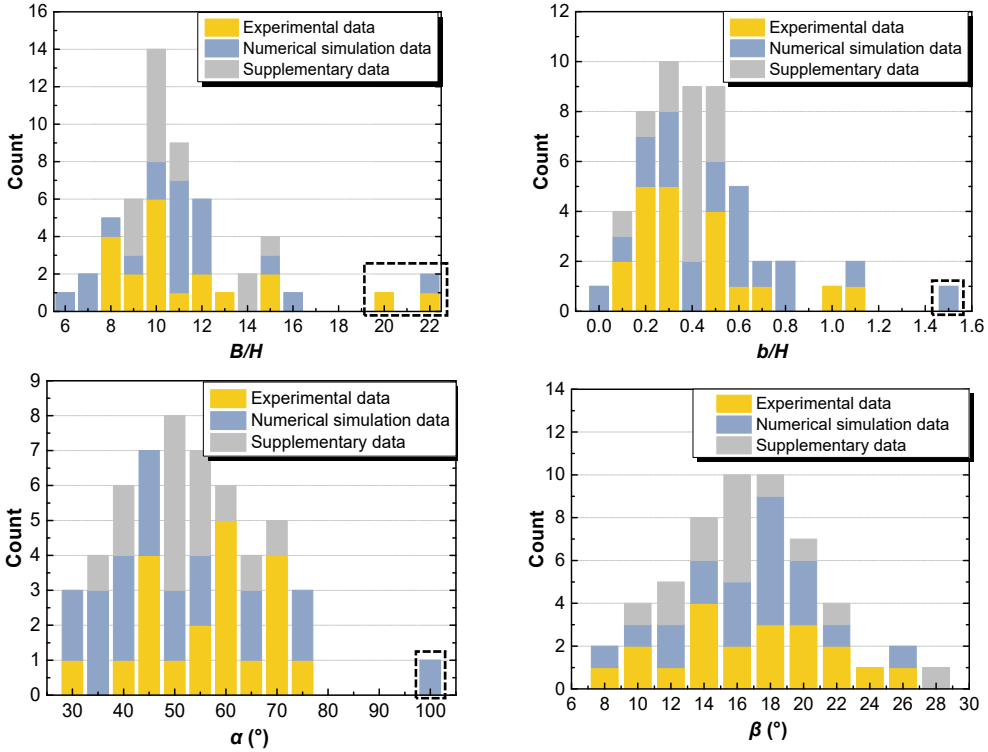

Figure 8. Cross-section distribution histogram of sample set.

4.3. Two-Dimensional CFD Numerical Simulation

In this paper, it was found through preliminary trial calculations that good prediction results could not be obtained when driven by 20 pure sets of wind tunnel test data or by 20 sets of numerical simulation data due to too little data. Under the mixed driving of two data modes, there may be significantly different underlying mapping relationships

between similar sections due to differences in recognition methods, making it difficult for machine learning models to distinguish them and obtain good prediction results. Therefore, the FDs of the existing 40 sets of cross-sections, as well as the 14 sets of supplementary cross-sections, are recalculated by CFD numerical simulation uniformly to obtain a new sample set more suitable for machine learning.

The numerical calculation domain is a two-dimensional flow field. Pointwise is used for geometric rendering and mesh generation, and ANSYS Fluent is used for numerical simulation. The Reynolds number of each sectional rigid model is the same as that of the corresponding wind tunnel test. In this paper, the FDs at 0° wind attack angle of each cross-section are calculated, and all the numerical simulation results are compared with the wind tunnel test results or calculation results by other researchers in the literature to check the validity of the data.

Figure 9 shows the results of 8 FDs for two of the 54 sets of cross-sections changing with the reduced wind speed under 0° wind attack angle. Figure 9a shows the comparison between the numerical simulation results and the wind tunnel test results of cross-section 1 from the database (as shown in Table 1). Figure 9b shows the comparison between the numerical simulation results in this study (CFD1) and other researcher's calculation results (CFD2) of cross-section 21 from the literature (as shown in Table 2) [37]. It can be seen from the figures that the numerical simulation results of these two closed-box girders are in good agreement with the wind tunnel test results and those of other researcher's calculations. This verification process is applicable to all other collected cross-sections. In the following, these numerical simulation data will be used for machine learning training and prediction so as to form an intelligent identification method for FDs of closed-box girders.

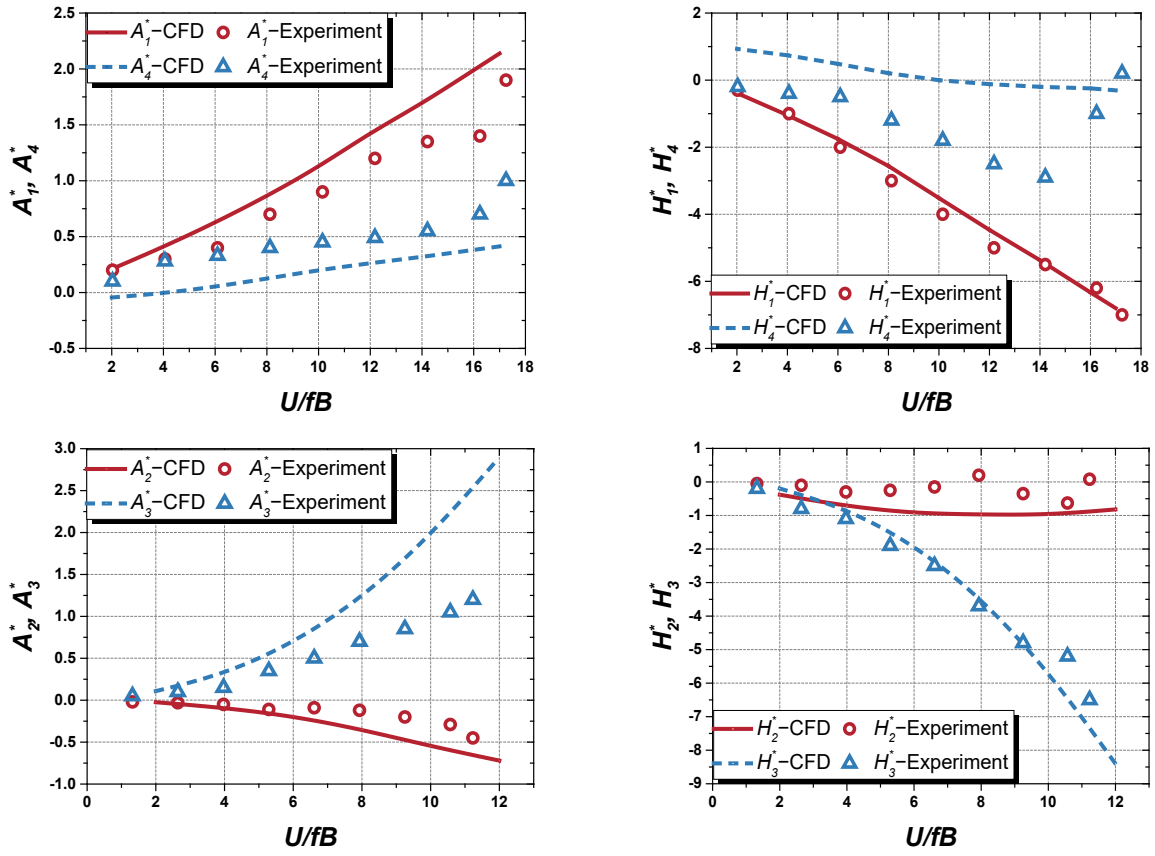

(**a**)

Figure 9. *Cont.*

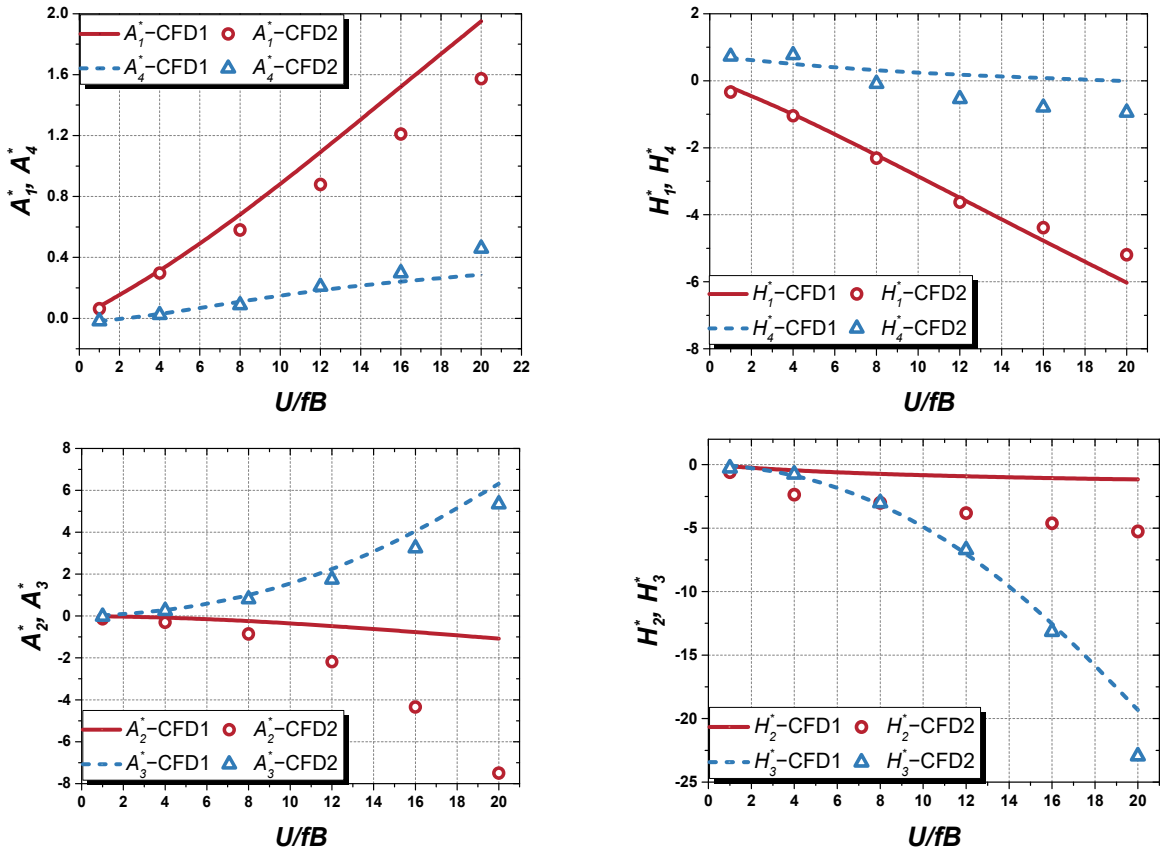

(**b**)

Figure 9. Trend of FDs changing with reduced wind speed: (**a**) the comparison between the numerical simulation results and the wind tunnel test results of cross-section 1; (**b**) the comparison between the numerical simulation results in this study (CFD1) and other researcher's calculation results (CFD2) of cross-section 21.

5. Intelligent Identification for FDs of Closed-Box Girders

This section focuses on the intelligent identification of FDs by GBDT. Firstly, the input and output of the machine learning model are introduced, and the data division pattern is also explained. Next, the training and prediction results of the model are presented. Finally, a post-interpretation is provided to further validate the effectiveness of the model.

5.1. Input and Output

When the machine learning method is used to study the aerodynamic characteristics of the bridge, the section geometry is a key factor, and the geometric dimensions of the cross-section must be used as the input for the neural network. For a closed-box girder, as shown in Figure 3, five parameters determine the unique cross-section, including B, H, b, α, and β. Since the amount of data is not big in this study, without being able to increase the amount of data significantly, the dimensionality of the input parameters should be reduced as much as possible. Considering that FDs are dimensionless parameters that are only related to the shape of the cross-section and are independent of the absolute size of the cross-section, four shape feature parameters (B/H, b/H, α, β), as well as reduced wind velocity, are finally used as input parameters for the model. The outputs of the model are FDs, but only one FD at a single reduced wind velocity is output each time. In addition, all inputs and outputs need to be pre-processed for normalization to reflect the essence of the data and avoid numerical problems before conducting machine learning training.

A regression analysis was performed before the machine learning training by creating an equation to determine how the dependent variable varies with multiple independent

variables and testing the equation and parameters for statistical significance. The T-test is used here for significance testing of the parameters, which can also be regarded as a parameter sensitivity analysis. When judging the regression analysis results, the effect of the corresponding variable is significant when $|t| > 2$, and the probability of error will not exceed 0.05. If $|t|$ is much greater than 2, the probability of error is even smaller. Table 4 gives the t-statistics of each input feature for the output parameter (FD). It can be seen that most of the values of $|t|$ are greater than 2, which proves that when the machine learning method is used to study the aerodynamic characteristics of bridges, the dimensions of cross-section and wind velocity are very important factors, and they must be used as inputs of the model.

Table 4. T-test of regression analysis.

***t*-Statistic**	A_1^*	A_4^*	H_1^*	H_4^*	A_2^*	A_3^*	H_2^*	H_3^*
B/H	2.539	1.237	−2.950	−3.798	−3.066	2.635	3.267	−2.977
b/H	−2.351	1.601	1.573	2.648	2.468	−1.829	−1.812	1.989
α	−4.517	1.407	1.632	2.681	2.802	−1.210	−1.079	1.277
β	4.147	−2.478	−1.033	−1.609	−2.339	0.847	0.380	−0.815
U/fB	115.834	47.381	−82.835	−27.241	−37.922	38.996	5.875	−37.282

5.2. Model Construction and Trial Calculation

The GBDT method used to identify FDs in this study is based on Python and its toolkit. The programming process is conducted on Jupyter Notebook which is a web-based interactive computing platform. After establishing the preliminary model, 20 sets of pure wind tunnel test data and 54 sets of hybrid data were used for trial calculations to evaluate the basic performance of the GBDT model. One of the evaluation indices of the model is fitting degree (R^2 statistic), which is defined as follows:

$$R^2(y, \hat{y}_i) = 1 - \frac{\sum_{i=1}^{n} (y_i - \hat{y}_i)^2}{\sum_{i=1}^{n} (y_i - \overline{y})^2}, \tag{11}$$

where y_i is the true value of the sample; $\hat{y}_i$ is the predicted value; and n is the number of samples. R^2 reflects the proportion of the variation in the dependent variables that can be explained by the independent variables through the regression relationship, and R^2 takes a value between [0,1]. The larger the R^2, the better the model.

To judge the prediction effect of trained machine learning models, the extrapolation ability of the test cross-section should also be evaluated, which is also called the generalization ability evaluation. The prediction accuracy can be reflected by the mean relative error (MRE), which is defined as follows:

$$MRE(y, \hat{y}) = \frac{1}{n} \sum_{i=1}^{n} \left| \frac{y_i - \hat{y}_i}{y_i} \right|, \tag{12}$$

where y_i is the true value of the sample; $\hat{y}_i$ is the predicted value; and n is the number of samples. The smaller the value of MRE, the more accurate the prediction.

Taking cross-section 1 as the test section, Figures 10 and 11 show the fitting degree and generalization ability of the model under two different datasets, and Table 5 gives the specific prediction errors. It can be seen that the GBDT model struggles to capture the potential distribution pattern of FDs under only 20 sets of wind tunnel test data. It is still unable to achieve very satisfactory prediction results under 54 sets of hybrid data after repeated hyperparameters tuning. To further test and improve the performance of the GBDT model, pure numerical simulation data is considered for subsequent model training and optimization.

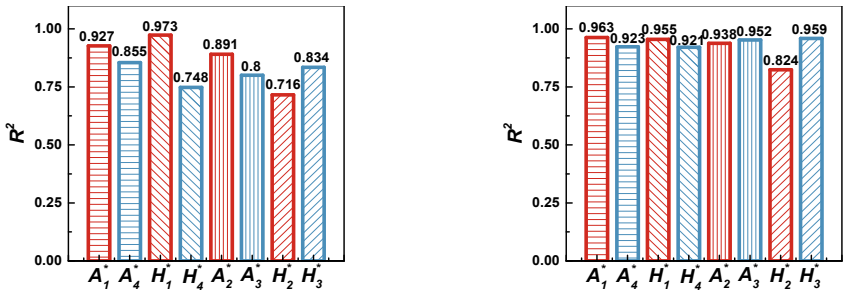

(**a**) (**b**)

Figure 10. Fitting degree of training set: (**a**) based on 20 sets of wind tunnel test data; (**b**) based on 54 sets of hybrid data.

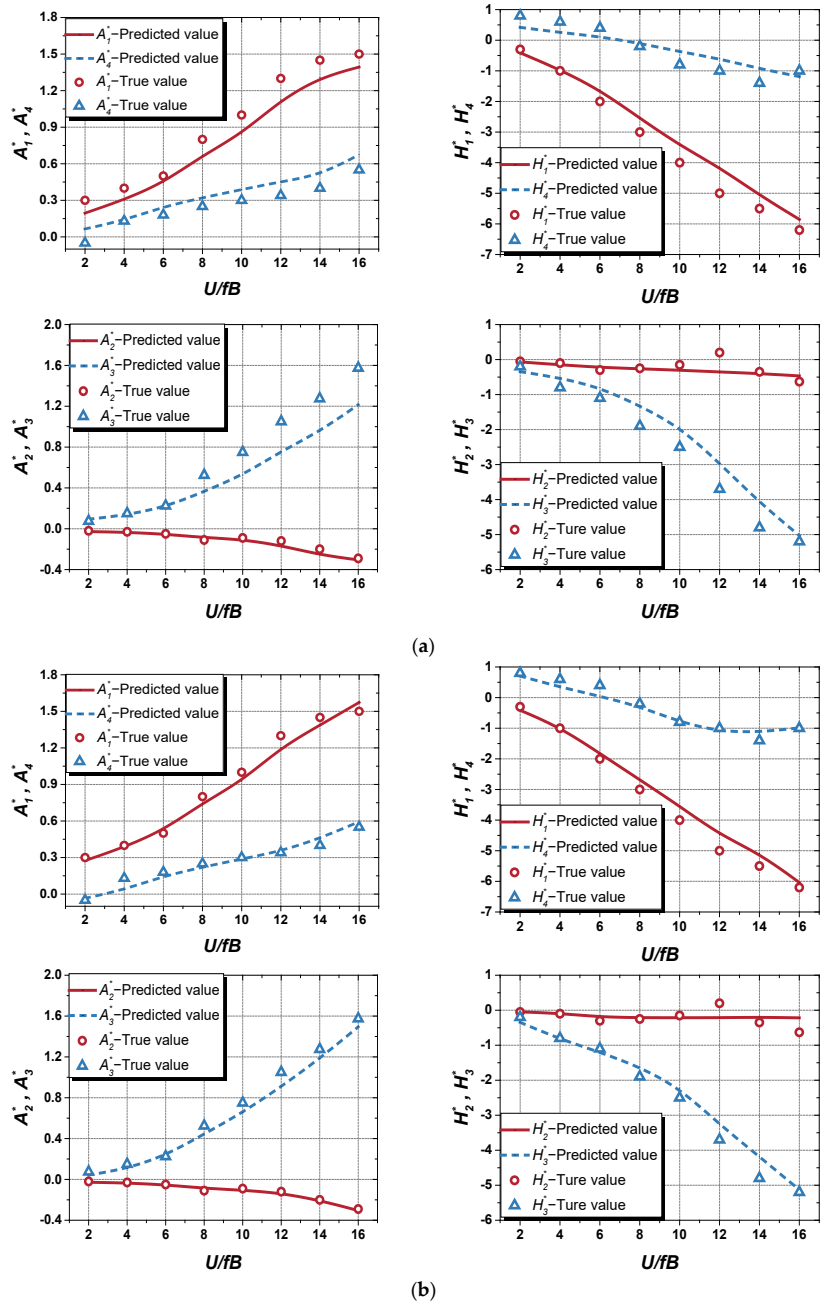

(**a**)

(**b**)

Figure 11. Prediction results of cross-section 1: (**a**) based on 20 sets of wind tunnel test data (model 1); (**b**) based on 54 sets of hybrid data (model 2).

Table 5. Prediction errors of cross-section 1.

MRE	A_1^*	A_4^*	H_1^*	H_4^*	A_2^*	A_3^*	H_2^*	H_3^*	Mean
Model 1	0.1656	0.5174	0.1491	0.4644	0.2105	0.2171	0.6673	0.2825	0.3342
Model 2	0.0595	0.2033	0.1150	0.2750	0.1480	0.1624	0.5310	0.1702	0.2081

5.3. Model Optimization and Validation

The ultimate goal of machine learning is to deploy trained models into real environments with the hope that the models can achieve good prediction effect in real scenarios. In this subsection, the training and prediction of GBDT models are based on pure numerical simulation data, and further analysis of GBDT model performance is given through complete cross validation.

5.3.1. Data Division

The sample set of machine learning is usually divided into three parts: training set; validation set; and test set. In this paper, cross validation is used to evaluate the accuracy and stability of the model through different data division patterns. Each sample will be used, in turn, as the training set, validation set, and test set. The cross validation method can help to monitor the changes of training effect under different patterns and avoid overfitting problems.

There are a total of 54 sets of pure numerical simulation data in this study. Since four samples were far from the mean of the datasets (samples in the dashed box in Figure 8, i.e., cross-section 10, 16, 24, and 37), they were removed from the sample set according to the statistical results. A total of 50 sets of data were available in the sample set. These 50 sets of data were used as the test set by turns, resulting in 50 working conditions. Under each working condition, we can take any one of the remaining 49 sets of samples as the validation set, and then all the remaining sets as the training set, resulting in 49 working conditions. This will ultimately result in a total of $50 \times 49 = 2450$ working conditions. The GBDT models are trained under all working conditions, from which the best and worst working conditions are displayed below to verify the applicability of the existing sample set for machine learning modeling under all working conditions.

5.3.2. Fitting Accuracy of Training Set

According to the data division pattern mentioned above, machine learning models were trained under 2450 working conditions. It can be found that the GBDT model always fits the training set with a high accuracy, regardless of the data division pattern used. The average training effect of FDs are shown in Figure 12. It can be seen from the figure that all the models can obtain the potential input–output transfer relationship of the training set. All values of R^2 are larger than 0.9 except for H_2^* and H_4^*.

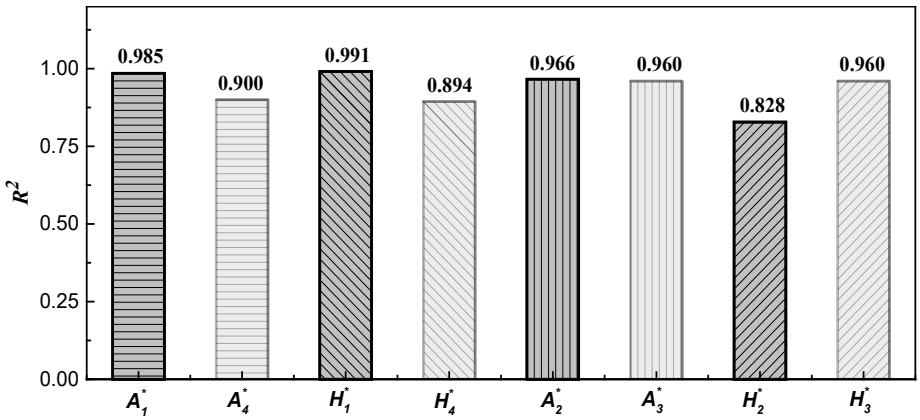

Figure 12. Average fitting degree.

5.3.3. Generalizability of Test Set

To verify the generalizability of models for the test cross-sections, the predicted value is compared with the true value, and Figure 13 gives the best and worst prediction outcomes for all test sets (predicted value means the predicted FD by the trained model; true value means the recalculated CFD result). Table 6 gives the specific errors of the best and worst predictions. It shows that the machine learning models are able to predict the distribution of FDs to a large extent under the current data condition.

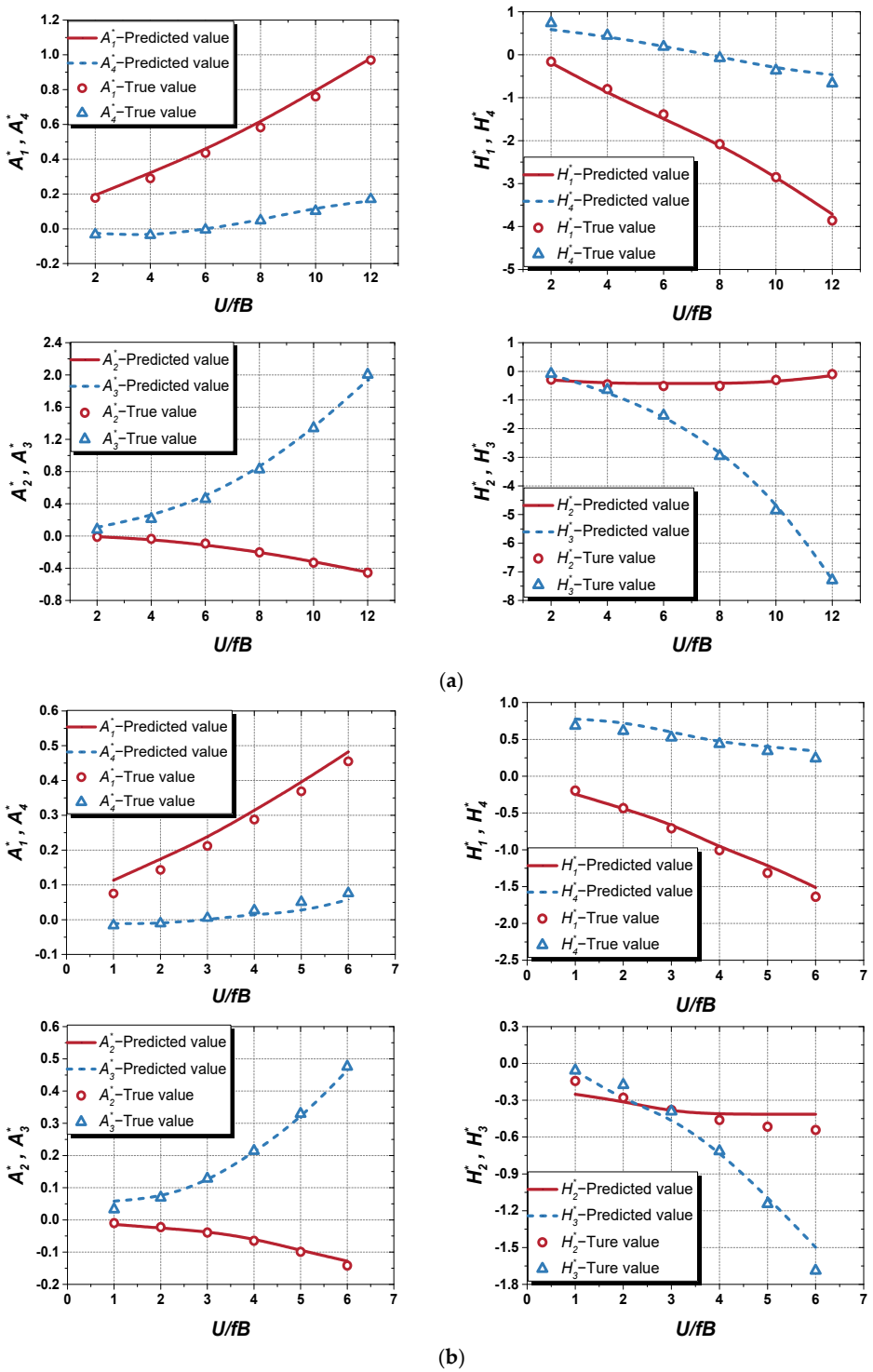

Figure 13. Generalization ability of test set: (**a**) the best prediction results (cross-section 29); (**b**) the worst prediction results (cross-section 26).

Table 6. Prediction errors of test set.

MRE	A_1^*	A_4^*	H_1^*	H_4^*	A_2^*	A_3^*	H_2^*	H_3^*	Mean
Best	0.0584	0.1745	0.0662	0.1924	0.0985	0.1089	0.2042	0.0833	0.1233
Worst	0.1755	0.4128	0.0910	0.1851	0.1411	0.1573	0.2400	0.1730	0.1970

5.4. Model Interpretation

The process of machine learning is often considered a "black box". The output is only obtained from the input, and the middle training process is difficult to explain. To express the machine learning model in some explicit way, the Shapley additive explanation (SHAP) is applied here. SHAP is an additive model interpreter constructed by Lundberg and Lee and inspired by cooperative game theory, which focuses on calculating the SHAP values of each feature as a reflection of how much the feature contributes to the prediction of the model [58]. SHAP interprets the predictive value of the model as the sum of SHAP values of each input feature:

$$\hat{y} = f_0 + \sum_{i=1}^{M} f_i, \tag{13}$$

where $\hat{y}$ is the predictive value; f_i is the SHAP value of each feature; and f_0 is the mean predictive value of all training samples. SHAP reflects the impact of each feature on the final prediction and can show the positivity and negativity of the impact, increasing the interpretability of the model. It also provides powerful data visualization functions to show the model and the prediction results, which are widely used to explain models with complex algorithms.

Figure 14 shows the SHAP values of shape parameters of the cross-section mentioned above (H, B, b, α, and β) for the prediction results of the model. They are ranked from top to bottom according to the effect magnitude on each FD. Overall, except H_2^*, the influence of these shape parameters on the other FDs is obvious. H, α, and β play a major role in the FDs, but the influence direction and the contribution degree of different shape parameters to the FDs are different. For $A_1^* \sim A_4^*$, H has the greatest effect on them. They have the same change direction as H. his means $A_1^* \sim A_4^*$ increase with the height of beam, but A_1^*, A_2^*, and A_3^* are more likely to be positive, and A_4^* is more likely to be negative. For $H_1^* \sim H_4^*$, the impact of β is large. Except that the situation of H_2^* is unclear, H_1^*, H_3^*, and H_4^* all change in the opposite direction to β, i.e., H_1^*, H_3^*, and H_4^* all decrease as the inclined web slope increases, and it is more likely that they are all negative. The specific contribution degree of these shape parameters to the FDs is given in a semi-quantitative form (SHAP values). SHAP analysis enables the interpretability of black box models, and it can even provide the necessary reference for further explicit representation of the training process of machine learning.

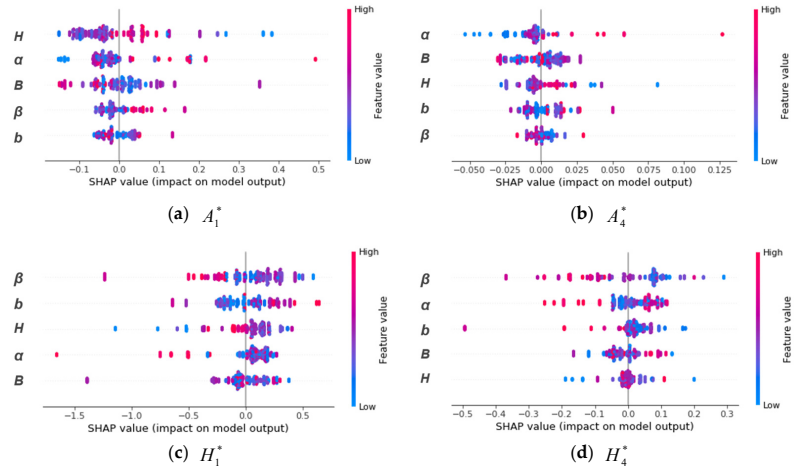

(**a**) A_1^* (**b**) A_4^*

(**c**) H_1^* (**d**) H_4^*

Figure 14. *Cont.*

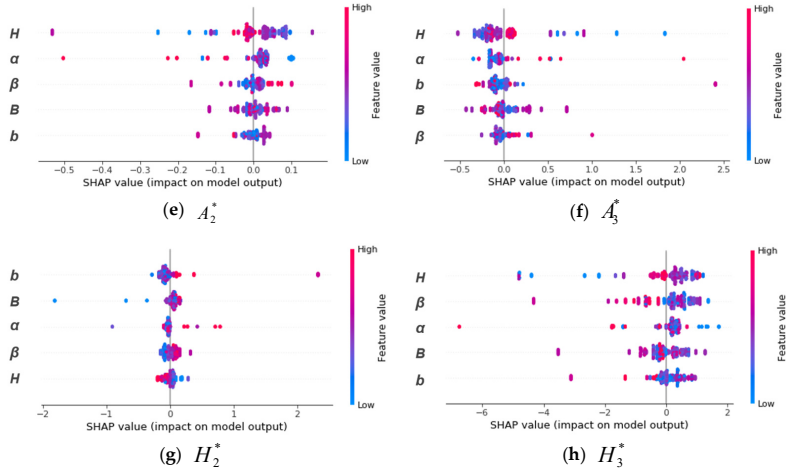

Figure 14. SHAP model explanation.

6. Prediction to Flutter Performance Analysis

The existing data-driven model can perform the identification of FDs out of physical and numerical wind tunnel tests to some extent. It can also provide a convenient and feasible option for expanding datasets of aerodynamic parameters. The FDs are dimensionless parameters related to the shape of the cross-section. When the shape of the cross-section changes, the FDs will inevitably be affected. In the process of calculating the CFV of a long-span bridge, by modifying the local size of the cross-section, the influence of the section shape on the CFV can be evaluated. At the same time, the machine learning model can be reasonably verified and optimized.

6.1. Intelligent Identification of Flutter Derivatives

This paper takes the Runyang Yangtze River Bridge (south branch) as an example, which is a suspension bridge with the main span of 1490 m. Figure 15 shows the cross-section diagram of main girder, and it is a steel streamlined closed-box girder with a height of 3 m and a width of 36.9 m.

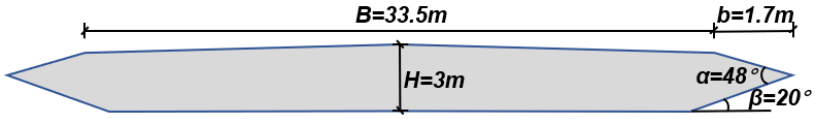

Figure 15. Cross-section diagram of Runyang Bridge.

The trained GBDT models under the best working condition are used to obtain the FDs of this main girder cross-section. The comparison of predictions with CFD calculations and experimental results are shown in Figure 16, and the specific prediction error (MRE) is shown in Table 7.

Table 7. Prediction error of Runyang Bridge.

MRE	A_1^*	A_4^*	H_1^*	H_4^*	A_2^*	A_3^*	H_2^*	H_3^*	Mean
CFD	0.0082	0.1401	0.1383	0.3958	0.0746	0.0435	0.2094	0.0109	0.1520
Experiment	0.1606	0.2113	0.1950	0.2174	0.1812	0.1828	0.2070	0.1445	0.1875

6.2. Sensitivity Analysis of Critical Flutter Velocity

This subsection analyzes the influence of FD prediction error on FCV calculation error and further analyzes the main source of error via sensitivity analysis of eight FDs.

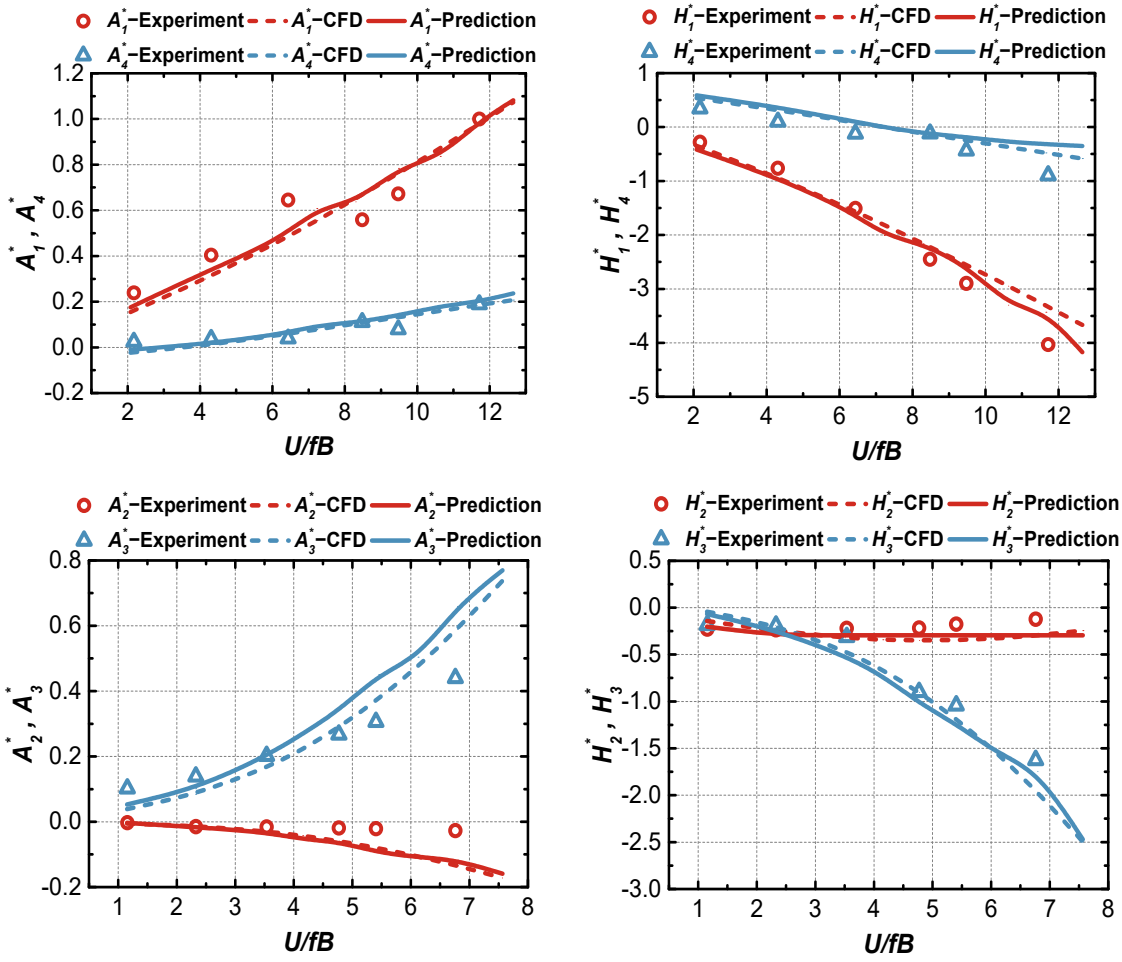

Figure 16. Prediction results of FDs for Runyang Bridge.

6.2.1. Prediction Error of Flutter Derivatives

As there are some errors in the FDs predicted by machine learning; we need to determine the extent to which these errors affect the CFV calculations before the aerodynamic shape sensitivity analysis. Using the predicted FDs of Runyang Bridge for the 2-D 3-DoF numerical analysis [59], the CFV of this structure at 0° wind attack angle can be obtained. Actually, several machine learning models based on different types of datasets (pure wind tunnel test datasets, pure numerical simulation datasets, hybrid datasets, etc.) were trained in this study. The FDs prediction results with different errors can be obtained by different trained models. These errors are ultimately reflected in the CFV calculation, as shown in Figure 17. It can be seen that even with an error of up to 25% in FDs prediction, the error in CFV calculation is only 10%. When the prediction error of FDs can be reduced to less than 15%, the calculation result of CFV is very close to the true value (measured by wind tunnel test), and the calculation error is less than 2%. This is due to the fact that different FDs have a major and minor effect on the CFV. If the prediction accuracy of important FDs is high, the CFV with high calculation accuracy can be obtained. It means there is no need to predict every FD accurately in the case of limited computing resources. This analysis further demonstrates that it is entirely feasible to identify FDs and perform flutter performance analysis by machine learning methods.

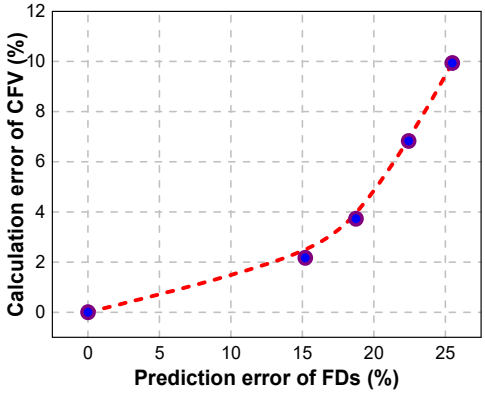

Figure 17. Error analysis. The x value of the blue dot represents the average error of the predicted FDs of each model, while the y value represents the calculation error of the corresponding CFV. The red dashed line indicates the overall trend of the CFV calculation error change with the FDs prediction error.

6.2.2. Sensitivity Analysis of Flutter Derivatives

For the cross-section shown in Figure 15, we can further analyze which FDs have a major impact on CFV by changing the magnitude of the FD sequentially. As shown in Figure 18, the horizontal axis represents the change ratio of FDs. $R > 1$ indicates the FD increases, and $R < 1$ indicates the FD decreases. The longitudinal axis indicates the change of CFV caused by parameter change. $R_V > 1$ indicates that the CFV increases after parameter change, and $R_V < 1$ indicates that the CFV decreases. It can be seen from the figure that the main factors affecting the CFV are A_1^*, A_2^*, A_3^*, and H_3^*. This conclusion is consistent with the test and analysis results of Hong from Tongji University [60]. A_1^* and H_3^* represent the coupled vertical motion speed excited by the aerodynamic lift generated by the torsional motion displacement and the aerodynamic damping formed by the aerodynamic moment caused by the feedback. They make the torsional vibration modal damping decrease from positive to negative, indicating that flutter has reached the critical state. A_2^* represents the aerodynamic damping formed by the aerodynamic moment directly generated by the torsional motion speed, and the increase in A_2^* with the increase in velocity will be beneficial to the stability of the system. The change of A_3^* also affects the CFV, but the influence is smaller than A_1^*, A_2^*, and H_3^*. The CFV decreases with the increase in A_1^*, A_3^*, and H_3^* and increases with the increase in A_2^*. The other FDs have almost no effect on the CFV. The conclusion above is not universal. It is only for the given cross-section and cross-sections with a similar shape and dimension.

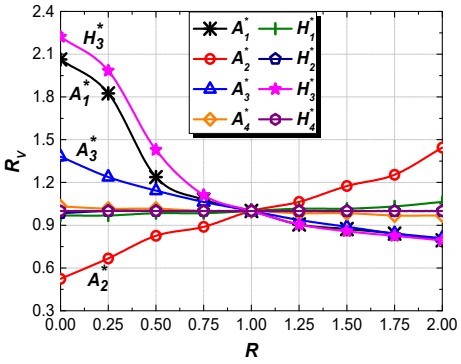

Figure 18. Influence of FDs on CFV.

6.3. Sensitivity Analysis of Aerodynamic Shape

The main factors affecting the flutter stability of bridges can be divided into two categories: (1) the aerodynamic shape of the cross-section, such as the width-to-height ratio, wind fairing angle, and inclined web slope; (2) the dynamic characteristics of the structure,

such as mass and frequency. The impact of these factors on the CFV is uncertain, and any parameter change can cause a change in the CFV.

This study does not consider the impact of dynamic characteristics on flutter stability currently, but only focuses on the impact of aerodynamic shape on flutter stability. Since CFV calculation can be combined with the machine learning prediction of FDs and high calculation accuracy can be obtained, the relationship between the shape of the cross-section and the CFV can be analyzed by the trained machine learning models. The analysis results can provide a reference for the aerodynamic shape optimization of the closed-box girder.

For closed-box girders, there are not many factors affecting the aerodynamic shape without considering the influence of the ancillary facilities on the CFV in the construction stage. It is time consuming, and it may not lead to better calculation results if every detail of the cross-section is taken into account. Therefore, this study only discusses three important parameters: width-to-height ratio; wind fairing angle; and inclined web slope.

6.3.1. Width-to-Height Ratio

The width-to-height ratio of a closed-box girder varies greatly. The width of cross-section varies from 30 m to 50 m and the height ranges from 2 m to 5 m. Taking the Runyang Bridge with the width-to-height ratio of 12.3 as an example, to reduce the workload of numerical calculation, it is assumed that the CFVs are proportional to different wind fairing angles and inclined web slopes, so the wind fairing angle and inclined web slope are kept unchanged. The width-to-height ratio is adjusted only by changing the width of the cross-section. The FDs with different width-to-height ratios are identified by the trained machine learning model, and the CFV under different width-to-height ratios is calculated by two-dimensional flutter numerical analysis. The result shows that the CFV decreases with the increase in the width-to-depth ratio, which is consistent with the conclusion obtained by Zhang of Chang'an University [61]. The variation law of CFV with the width-to-depth ratio and the comparison with Zhang's analysis are shown in Figure 19a. In this study, it can also be found that the CFV decreases sharply when the width-to-height ratio is lower than 11, and the decrease trend of CFV gradually slows down with the increase in the width-to-depth ratio when the ratio is greater than 11.

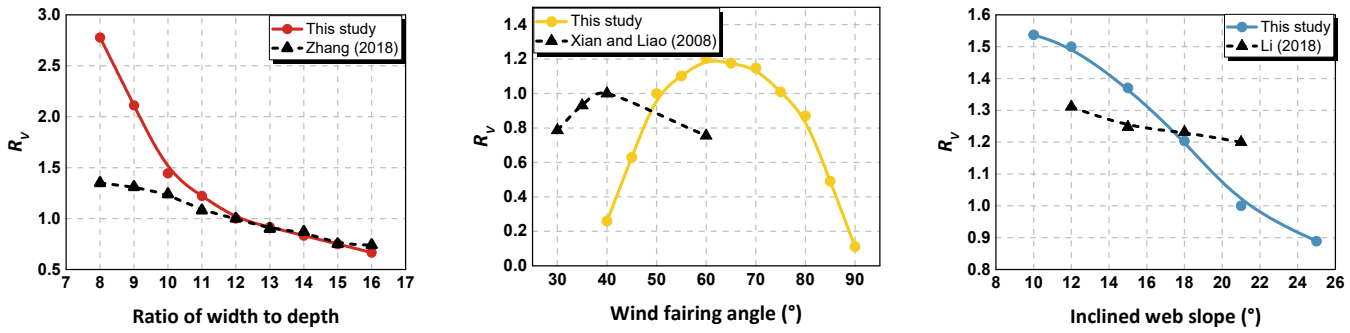

(**a**) (**b**) (**c**)

Figure 19. Influence of shape parameters on CFV: (**a**) width-to-height ratio [61]; (**b**) wind fairing angle [62]; (**c**) inclined web slope [63].

6.3.2. Wind Fairing Angle

Figure 19b shows the CFV changing with the wind fairing angle. It can be seen that the CFV first increases and then decreases with the increase in the wind fairing angle and reaches the peak at around 60°. Xian and Liao designed several wind fairings with different angles for a closed-box girder and analyzed the impact of the wind fairing angle on the CFV based on wind tunnel test [62]. The result showed that the CFV first increased and then decreased with the increase in wind fairing angle (α) (i.e., from 30° to 60°). This trend is consistent with the results obtained in this study ($40° < \alpha < 90°$). The experimental result of a wind fairing angle larger than 60° is not given by Xian and Liao. Since the shape

dimensions of the closed-box girder in their study are somewhat different from those in this paper, the optimal wind fairing angles are also different. Although the conclusion is limited, which is only applicable to the closed-box girder section with a specific width-to-depth ratio and inclined web slope, the influence regularity of the wind fairing angle on CFV can still be used as a reference for the optimization of aerodynamic shape.

6.3.3. Inclined Web Slope

Li et al. studied the influence of inclined web slope on CFV by wind tunnel tests [63]. The conclusion is that for a closed-box girder with the width-to-depth ratio of 11, the larger the inclined web slope is, the smaller the CFV is. For the closed-box girder with the width-to-depth ratio of 7, the influence of inclined web slope on CFV is very small. The width-to-depth ratio of the prototype structure in this paper (the main girder cross-section of Runyang Bridge shown in Figure 15) is 12.3. When the inclined web slope is changed from 10° to 25°, the influence regularity of inclined web slope on CFV is shown in Figure 19c. It can be seen that the CFV decreases with the increase in inclined web slope, which is consistent with Li's research, and this trend is almost linear. However, during the actual design and construction, the specific inclined web slope should be determined according to the actual engineering because it will significantly increase the manufacturing difficulty if the inclined web slope is too small.

7. Conclusions

In this paper, based on a database of flutter derivatives obtained by wind tunnel tests and numerical simulation, the flutter derivatives of closed-box girders are identified by machine learning methods. Modeling is implemented with a gradient boosting decision tree algorithm. The model is trained and analyzed under different data division patterns, and model interpretation after training is realized. The sensitivity of flutter derivatives and the influence of the geometric shape of the cross-section on critical flutter velocity are also analyzed, which provides a reference for aerodynamic shape optimization and further verifies the validity of the models. Some conclusions are summarized as follows:

- The model trained by gradient boosting decision tree is able to predict the flutter derivatives under different data division patterns with the mean relative error of less than 0.2. The machine learning prediction error of flutter derivatives will be weakened in the numerical calculation of critical flutter velocity. If the prediction error of flutter derivatives can be reduced to less than 15%, the calculation result of critical flutter velocity will be very close to the true value (i.e., the calculation error is less than 2%).
- For closed-box girders, A_1^*, A_2^*, A_3^*, and H_3^* have great influence on critical flutter velocity. The critical flutter velocity decreases with the increase in A_1^*, A_3^*, and H_3^* and increases with the increase in A_2^*. The other flutter derivatives almost do not affect the critical flutter velocity. This conclusion is not universal; it is only applicable for the prototype structure in this study or for cross-sections with similar shape dimensions.
- The critical flutter velocity decreases with the increase in the width-to-depth ratio of the closed-box girder. In the range of 40°–90° of wind fairing angles, the critical flutter velocity first increases and then decreases with the increase in angle and reaches the peak at around 60°. The critical flutter velocity decreases with an increase in inclined web slope and is almost linear for a particular width-to-height ratio.

The machine learning method proposed in this paper can provide a new means of identifying flutter derivatives and rapidly evaluating flutter stability in the preliminary wind-resistant design stage. However, this study has some limitations:

- The proposed methods are only applicable to closed-box girder cross-sections, and the sensitivity analysis of the critical flutter wind speed with the shape of cross-sections only focuses on three feature dimensions: width-to-height ratio; wind fairing angle; and inclined web slope. In the future, we expect to implement more refined research

on the change of shape and even on the ancillary facilities of the main girder and expand the research to other types of main girder cross-sections.

- The identification method of flutter derivatives proposed in this paper can achieve rapid evaluation of flutter stability without physical and numerical wind tunnel tests, but a good prediction effect can only be achieved based on pure numerical simulation data at present. It is necessary to further improve the accuracy and robustness of intelligent identification and achieve machine learning predictions based on complete wind tunnel test data, which depends on larger datasets and better data conditions.
- The existing data and proposed methods only achieve the identification of eight flutter derivatives and two-dimensional flutter stability analysis. In the future, more works on three-dimensional flutter stability analysis based on the predicted eighteen flutter derivatives via machine learning methods will also be needed.

Author Contributions: Conceptualization, Y.G. and C.B.; Methodology, Y.G.; Investigation, N.C.; Data curation, N.C.; Writing—original draft, N.C.; Writing—review and editing, Y.G. and C.B.; Supervision, Y.G. and C.B.; Funding acquisition, Y.G. All authors have read and agreed to the published version of the manuscript.

Funding: This research was funded by the National Natural Science Foundation of China (51978527, 52278520) and China Scholarship Council (201906260198).

Data Availability Statement: The data presented in this study are available on request from the corresponding author.

Acknowledgments: The authors gratefully acknowledge the technical support of the University of Florence. We also appreciate the writing suggestions from Genshen Fang and the computational assistance provided by Yizhe Lan, Zihang Liu, and Miaomiao Wei.

Conflicts of Interest: The authors declare no conflict of interest.

References

1. Xiang, H.F.; Ge, Y.J. Aerodynamic Challenges in Span Length of Suspension Bridges. *Front. Archit. Civ. Eng. China* **2007**, *1*, 153–162. [CrossRef]
2. Liu, S.Y.; Zhao, L.; Fang, G.S.; Hu, C.X.; Ge, Y.J. Numerical Aerodynamic Characteristics and Modeling of a Quasi-Flat Plate at Torsional Vibration: Effects of Angle of Attack and Vibration Amplitude. *Nonlinear Dyn.* **2022**, *107*, 2027–2051. [CrossRef]
3. Fang, G.S.; Cao, J.X.; Yang, Y.X.; Zhao, L.; Cao, S.Y.; Ge, Y.J. Experimental Uncertainty Quantification of Flutter Derivatives for a PK Section Girder and Its Application on Probabilistic Flutter Analysis. *J. Bridge Eng.* **2020**, *25*, 04020034. [CrossRef]
4. Qin, X.R.; Gu, M. Stochastic System Method for Identification of Aerodynamic Derivatives of Bridge Decks in Turbulent Flow. *China Civ. Eng. J.* **2005**, *38*, 73–77. (In Chinese) [CrossRef]
5. Sarkar, P.P.; Jones, N.P.; Scanlan, R.H. Identification of Aeroelastic Parameters of Flexible Bridges. *J. Eng. Mech.* **1994**, *120*, 1718–1742. [CrossRef]
6. Ding, Q.S.; Zhou, Z.Y.; Zhu, L.D.; Xiang, H.F. Identification of Flutter Derivatives of Bridge Decks with Free Vibration Technique. *J. Wind. Eng. Ind. Aerodyn.* **2010**, *98*, 911–918. [CrossRef]
7. Xu, F.Y.; Zhu, L.D.; Ge, X.M.; Zhang, Z. Some New Insights into the Identification of Bridge Deck Flutter Derivatives. *Eng. Struct.* **2014**, *75*, 418–428. [CrossRef]
8. Yamada, H.; Miyata, T.; Ichikawa, H. Measurement of Aerodynamic Coefficients by System Identification Methods. *J. Wind. Eng. Ind. Aerodyn.* **1992**, *41*, 1255–1263. [CrossRef]
9. Chowdhury, A.G.; Sarkar, P.P. A New Technique for Identification of Eighteen Flutter Derivatives Using a Three-degree-of-freedom Section Model. *Eng. Struct.* **2003**, *25*, 1763–1772. [CrossRef]
10. Borri, C.; Costa, C. Quasi-steady Analysis of a Two-dimensional Bridge Deck Element. *Comput. Struct.* **2004**, *82*, 993–1006. [CrossRef]
11. Borri, C.; Zahlten, W. Fully Simulated Nonlinear Analysis of Large Structures Subjected to Turbulent Artificial Wind. *Mech. Struct. Mach.* **1991**, *19*, 213–250. [CrossRef]
12. Borri, C.; Höffer, R. Aeroelastic Wind Forces on Flexible Bridge Girders. *Meccanica* **2000**, *35*, 1–15. [CrossRef]
13. Fang, G.S.; Pang, W.; Zhao, L.; Rawal, P.; Cao, S.Y.; Ge, Y.J. Toward a Refined Estimation of Typhoon Wind Hazards: Parametric Modeling and Upstream Terrain Effects. *J. Wind. Eng. Ind. Aerodyn.* **2021**, *209*, 104460. [CrossRef]
14. Hu, X.N.; Fang, G.S.; Yang, J.Y.; Zhao, L.; Ge, Y.J. Simplified Models for Uncertainty Quantification of Extreme Events Using Monte Carlo Technique. *Reliab. Eng. Syst. Saf.* **2023**, *230*, 108935. [CrossRef]

15. Zhu, Z.W.; Gu, M. Wind Tunnel and CFD Study on Identification of Flutter Derivatives of a Long-span Self-anchored Suspension Bridge. *Comput. Aided Civ. Infrastruct.* **2007**, *22*, 541–554. [CrossRef]
16. Wang, X.J. Identification of Aerodynamic Parameters of Bridge Decks by Stochastic Approaches. Ph.D. Thesis, Tongji University, Shanghai, China, 2008. (In Chinese) [CrossRef]
17. Xu, F.Y.; Zhang, Z.B. Free Vibration Numerical Simulation Technique for Extracting Flutter Derivatives of Bridge Decks. *J. Wind. Eng. Ind. Aerodyn.* **2017**, *170*, 226–237. [CrossRef]
18. Zhou, Y.; Kijewski, T.; Kareem, A. Aerodynamic Loads on Tall Buildings: Interactive Database. *J. Struct. Eng.* **2003**, *129*, 394–404. [CrossRef]
19. Wang, J.; Cheng, J.; Teng, E. Design Wind Loads on Tall Buildings: A Wind Tunnel Data Based Expert System Approach. In Proceedings of the 11th International Conference on Wind Engineering, Lubbock, TX, USA, 2–5 June 2003.
20. Ho, T.; Surry, D.; Morrish, D.; Kopp, G. The UWO Contribution to the NIST Aerodynamic Database for Wind Loads on Low Buildings: Part 1. Archiving Format and Basic Aerodynamic Data. *J. Wind. Eng. Ind. Aerodyn.* **2005**, *93*, 1–30. [CrossRef]
21. Quan, Y.; Tamura, Y.; Matsui, M.; Cao, S.Y. Introduction to Aerodynamic Database of Low Buildings. In Proceedings of the 7th National Conference on Wind Engineering and Industrial Aerodynamics, Chengdu, China, 1–3 August 2006. (In Chinese).
22. Jung, S.; Ghaboussi, J.; Kwon, S.D. Estimation of Aeroelastic Parameters of Bridge Decks Using Neural Networks. *J. Eng. Mech.* **2004**, *130*, 1356–1364. [CrossRef]
23. Chen, C.H.; Wu, J.C.; Chen, J.H. Prediction of Flutter Derivatives by Artificial Neural Networks. *J. Wind. Eng. Ind. Aerodyn.* **2008**, *96*, 1925–1937. [CrossRef]
24. Lute, V.; Upadhyay, A.; Singh, K.K. Support Vector Machine Based Aerodynamic Analysis of Cable Stayed Bridges. *Adv. Eng. Softw.* **2009**, *40*, 830–835. [CrossRef]
25. Chung, J.; Lee, S.W.; Chang, S.; Kim, Y.S. Estimation of Flutter Derivatives of Various Sections Using Numerical Simulation and Neural Network. In Proceedings of the 2012 World Congress on Advances in Civil, Environmental, and Materials Research, Seoul, Republic of Korea, 26–30 August 2012.
26. Rizzo, F.; Caracoglia, L. Artificial Neural Network Model to Predict the Flutter Velocity of Suspension Bridges. *Comput. Struct.* **2020**, *233*, 106236. [CrossRef]
27. Abbas, T.; Kavrakov, I.; Morgenthal, G.; Lahmer, T. Prediction of Aeroelastic Response of Bridge Decks Using Artificial Neural Networks. *Comput. Struct.* **2020**, *231*, 106198. [CrossRef]
28. Mei, H.Y. Deep Neural Network-Based Method for Calculating Nonlinear Aerodynamic Forces and Responses of Bridge Section. Ph.D. Thesis, Southwest Jiaotong University, Chengdu, China, 2021. (In Chinese) [CrossRef]
29. Li, Y.; Li, C.; Liang, Y.D.; Li, J.W. Fast Prediction of the Flutter Critical Wind Speed of Streamlined Box Girders by Using Aerostatic Force Coefficients and Artificial Neural Networks. *J. Wind. Eng. Ind. Aerodyn.* **2022**, *222*, 104939. [CrossRef]
30. Li, H.; Spencer, B.F.; Bao, Y. Machine Learning Paradigm for Structural Health Monitoring. *Struct. Health Monit.* **2021**, *20*, 1353–1372. [CrossRef]
31. Scanlan, R.H.; Tomko, J.J. Airfoil and Bridge Deck Flutter Derivatives. *J. Eng. Mech.* **1971**, *6*, 1717–1737. [CrossRef]
32. Gu, M.; Zhang, R.; Xiang, H. Identification of Flutter Derivatives of Bridge Decks. *J. Wind. Eng. Ind. Aerodyn.* **2000**, *84*, 151–162. [CrossRef]
33. Li, Y.; Liao, H.; Qiang, S. Weighting Ensemble Least-square Method for Flutter Derivatives of Bridge Decks. *J. Wind. Eng. Ind. Aerodyn.* **2003**, *91*, 713–721. [CrossRef]
34. Bartoli, G.; Contri, S.; Mannini, C.; Righi, M. Toward an Improvement in the Identification of Bridge Deck Flutter Derivatives. *J. Eng. Mech.* **2009**, *135*, 771–785. [CrossRef]
35. Chen, N.Y.; Ge, Y.J. Aerodynamic Parameter Identification of Typical Bridge Sections Based on Artificial Neural Network. *China Civ. Eng. J.* **2019**, *52*, 91–97. (In Chinese) [CrossRef]
36. Chen, N.Y. Database Integration and Intelligent Evaluation of Wind-resistant Performances of Long-Span Bridges. Master's Thesis, Tongji University, Shanghai, China, 2017. (In Chinese).
37. Wang, X. Numerical Simulation Study on Wind-induced Vibration of Long-span Bridges. Master's Thesis, Guizhou University, Guiyang, China, 2018. (In Chinese).
38. Zhang, Q. Research on Flutter Derivatives of Bridge Girder Sections by Numerical Simulation. Master's Thesis, Southwest Jiaotong University, Chengdu, China, 2008. (In Chinese).
39. Zhu, A.D. Wind-resistant Performance Analysis and Experimental Investigation on Long-span Cable-stayed Bridges. Master's Thesis, Dalian University of Technology, Dalian, China, 2014. (In Chinese).
40. Zhang, Z.B. Numerical Study on Nonlinear Aerodynamic Forces on Typical Bridge Decks. Master's Thesis, Dalian University of Technology, Dalian, China, 2016. (In Chinese).
41. Qi, Y.H. Numerical Analysis on 3D Flutter Instability of Long-span Suspension Bridges and Effects from Active Controlled Wind Barrier. Master's Thesis, Central South University, Changsha, China, 2013. (In Chinese) [CrossRef]
42. Bai, H.; Xia, Y.; Liu, J.X.; Li, J.W. Numerical Simulation for Flutter Stability of Streamlined Bridge Decks. *J. Chang. Univ.* **2011**, *31*, 45–50. (In Chinese) [CrossRef]
43. Hong, G. Identifying Long-Span Bridge Flutter Derivatives via the Free Vibration Method Based on the Flutter Software. Master's Thesis, Chang'an University, Xi'an, China, 2012. (In Chinese) [CrossRef]

44. Zhu, Y.Q. Numerical Simulation and Experimental Study on Flutter Characteristics of Long Span Suspension Bridge. Master's Thesis, Southwest Jiaotong University, Chengdu, China, 2017. (In Chinese).
45. Bai, Y.L.; Ou, J.P. Numerical simulation of flutter derivatives of CFRP streamlined box girders and determination of critical wind speed. In Proceedings of the 14th National Conference on Structural Wind Engineering, Beijing, China, 27–28 August 2009. (In Chinese).
46. Hao, D. The Study of the Effect of Tuyere on Bridge Flutter Stability. Master's Thesis, Chang'an University, Xi'an, China, 2011. (In Chinese) [CrossRef]
47. Jiao, L.N. The Effects of Characteristics of Mean Wind and Fluctuate Wind on Long-span Bridge. Master's Thesis, Harbin Institute of Technology, Harbin, China, 2009. (In Chinese).
48. Fu, J. Wind Tunnel Experimental Investigation and Numerical Simulation on the Flutter Characteristic of a Long-span Suspension Bridge. Master's Thesis, Chongqing University, Chongqing, China, 2016. Available online: https://kns.cnki.net/KCMS/detail/detail.aspx?dbname=CMFD201701&filename=1016908037.nh (accessed on 1 September 2022). (In Chinese).
49. Peng, Y. The Numerical Analysis for Flutter Stability on Streamlined Box Girder and Pneumatic Control Measures. Master's Thesis, Central South University, Changsha, China, 2012. (In Chinese).
50. Gao, W. Flutter Derivatives Research of Large Span Bridges under Skew Wind. Master's Thesis, Southwest Jiaotong University, Chengdu, China, 2013. (In Chinese) [CrossRef]
51. Pang, W. The Identification of Flutter Derivatives for Long-Span Bridges Based on Fluent. Master's Thesis, Southwest Jiaotong University, Chengdu, China, 2007. (In Chinese) [CrossRef]
52. Hong, C.J. Numerical Calculation Method for Flutter Critical Wind Speed and Flutter Derivatives of Long-Span Bridge Streamlined Steel Box Girder. Master's Thesis, Southwest Jiaotong University, Chengdu, China, 2019. (In Chinese) [CrossRef]
53. Lv, L.S.; Meng, Q.B.; Li, T. Study on Flutter Derivative Identification Method Based on MIMO System. *Bridge Tunn. Eng.* **2011**, *2*, 42–47. (In Chinese)
54. Wang, D.L. Numerical Simulation of Aeroelastic Problems on Bridges Based on Discrete Vortex Method. Master's Thesis, Tongji University, Shanghai, China, 2003. (In Chinese).
55. Xia, Y. Numerical Calculation of the Flutter Stability for Long-span Suspension Bridge. Master's Thesis, Chang'an University, Xi'an, China, 2011. (In Chinese) [CrossRef]
56. Chao, C.R. Research on Flutter Bridges with Three Towers and Its Whole Process Simulation. Master's Thesis, Southeast University, Nanjing, China, 2015. (In Chinese).
57. Chen, Y.Q. Aerodynamic Shape Optimization of Central Slotted Box Girders Based on Performance of Wind-induced Self-excited Vibration. Master's Thesis, Tongji University, Shanghai, China, 2016. (In Chinese).
58. Lundberg, S.M.; Lee, S.I. A Unified Approach to Interpreting Model Predictions. In Proceedings of the 31st International Conference on Neural Information Processing Systems, Long Beach, CA, USA, 25 November 2017. [CrossRef]
59. Zhu, Z.W.; Chen, Z.Q. Numerical Simulations for Aerodynamic Derivatives and Critical Flutter Velocity of Bridge Deck. *China J. Highw. Transp.* **2004**, *17*, 41–45. (In Chinese) [CrossRef]
60. Hong, L.Z. Influence of Wind Barrier on Flutter Performance of Bridge. Master's Thesis, Tongji University, Shanghai, China, 2020. (In Chinese).
61. Zhang, H. Estimation for Critical Flutter Velocity of the Bridge with Flat Box Girder. Master's Thesis, Chang'an University, Xi'an, 2018. Available online: https://kns.cnki.net/KCMS/detail/detail.aspx?dbname=CMFD201901&filename=1018791251.nh (accessed on 1 September 2022). (In Chinese).
62. Xian, R.; Liao, H.L. Wind Tunnel Test Study of Aerodynamic Optimization Measures for Flutter Stability of Critical Flat Steel Box Girder. *World Bridges* **2008**, *138*, 44–47. (In Chinese)
63. Li, Z.G.; Wang, Q.; Liao, H.L.; Wei, Y.F. Effects of Inclined Web Slope on Flutter Performance of Flat Box Girders and Their Quantification. *J. Vib. Shock.* **2018**, *37*, 17–24. (In Chinese) [CrossRef]